Contents

Electronic Supplementary Information (ESI)

Jeehyun Yang[a], Mica C. Smith[b], Matthew B. Prendergast[b], Te-Chun Chu[b], William H. Green[b,*]

[a]*Department of Earth, Atmospheric and Planetary Sciences, Massachusetts Institute of Technology, Cambridge, MA 02139, United States*
[b]*Department of Chemical Engineering, Massachusetts Institute of Technology, Cambridge, MA 02139, United States*

1. INTRO

In order to make it easier for readers to connect the supplementary information to the main text, supplementary information here are grouped to the related section in the main text

*Corresponding author
Email address: whgreen@mit.edu (William H. Green)

2. SI related to EXPERIMENTAL

2.1. H-NMR analyses of iodonaphthalene precursors

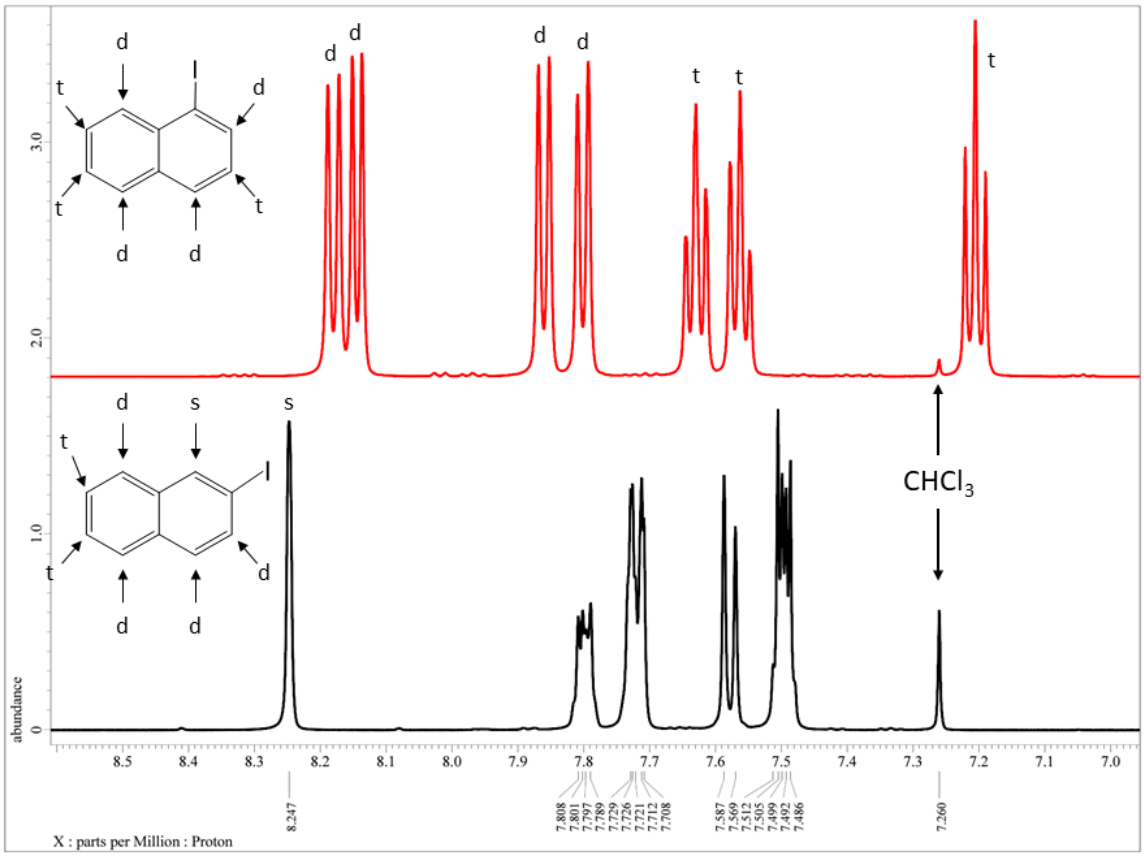

Figure S 1: The top red spectra is H-NMR spectra of 1-iodonaphthalene of 97% purity. The bottom black spectra is H-NMR spectra of 2-iodonaphthalene of >98% purity

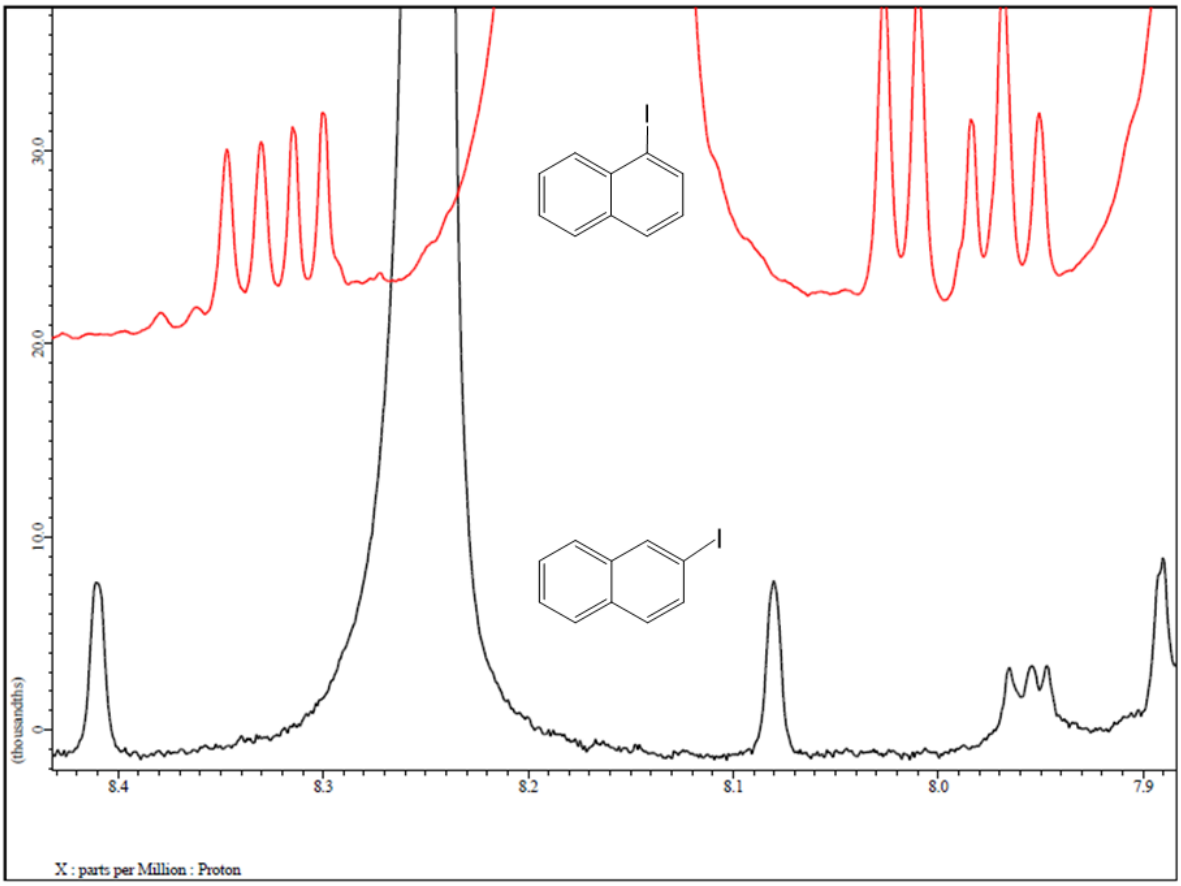

Figure S 2: Enlarged H-NMR spectra between 7.89 and 8.43, where the top red spectrum is of 1-iodonaphthalene (97%) and the bottom black spectrum is of 2-iodonaphthalene (>98% purity)

2.2. Control experiments: The photolysis of various precursors without C_2H_2

The signals at m/z = 126, 127, 128, and 254 appeared after the photolysis of each radical precursor ($C_{10}H_7I$) with no acetylene (C_2H_2). The small signal at m/z = 126 showed similar time-dependent behavior to m/z = 127 (Figure S3), which might indicate that m/z = 126 is a product from dissociative ionization where ionization of m/z = 127 photolysis product leads to some fragmentation into m/z = 126 and H atom. The m/z = 254 signal mainly corresponds to the 1- (or 2-) iodonaphthalene precursor (IE = 8.03 eV).[1], while I_2 and $C_{20}H_{14}$ might partially contribute to the m/z =254 signals after photolysis. The m/z = 127 and 128 signals are consistent with the naphthalenyl radical and naphthalene, but also I-atom and HI. The literature IEs for naphthalene, I-atom, and HI are 8.144 eV, 10.451 26 eV, and 10.386 eV, respectively,[2] and lower than the energy of the PI laser (10.49 eV). In Figure S3, the measured time-dependent mass signal at m/z = 127 and 128 is shown with the ratio of m/z = 128 to m/z = 127 (Figure S3b). The main photolysis channel is $C_{10}H_7$ + I; both of these species have m/z = 127. The rise time of the m/z = 127 signal is apparently due to diffusion of the radicals across the narrow gap from the photolyzed region to the sampling pinhole; this rise time is sensitive to alignment of the photolysis laser.

Several different processes affect the ratio of the m/z = 128 to m/z = 127 signals. At long times most of the naphthalenyl radicals are expected to have reacted away, primarily by recombination, so the m/z = 127 signal is expected to be predominantly due to the less-reactive iodine atoms. The I atoms also are moderately reactive, so as expected the m/z = 127 signal drops off at the longest times, causing the 128/127 ratio to rise. At the shortest time points, the m/z = 127 signal is a sum of naphthalenyl radical + I atom, with the I atom being more important because of its high PICS. The very small m/z = 128 signal at the earliest times indicates that the direct photolytic production of HI + $C_{10}H_6$ is negligible, consistent with the very small signal observed at m/z = 126. Some of that very small m/z = 128 signal seen at the earliest times is likely due to ^{13}C isotopomer of $C_{10}H_7$.

The m/z = 128 signal rises rapidly around 1 ms up to a peak around 2 ms after the photolysis pulse. We believe that this rapid increase in signal is primarily caused by $C_{10}H_7$ radicals abstracting an H atom at the sampling pinhole as discussed in the main text (referred to as pinhole reaction). The m/z = 128 signal due to this process peaks and declines as the concentration of $C_{10}H_7$ radicals drops due to recombination. However, there is a residual m/z = 128 signal at longer times when the $C_{10}H_7$ concentration is very small. Some of this is stable naphthalene $C_{10}H_8$ formed by wall reactions inside the reactor or $C_{10}H_7$ + $C_{10}H_7$ disproportionation reactions in the gas phase, and some is stable HI formed from $C_{10}H_7$ + I disproportionation, all at earlier times when the $C_{10}H_7$ concentration was high. Some is also HI formed from I atoms abstracting an H from the wall of the reactor. A portion of the m/z = 128 signal could be from I atoms abstracting an H atom from the pinhole as they exit towards the mass spec. However, surely not all of the m/z = 128 signal could be due to that process, since in that case the 128/127 ratio would stay constant and the 128 signal would drop in concert with the 127 signal at long times, different from what was observed. From analyzing the data shown in Figure S3a, less than 25% of the I atoms react in the sampling pinhole.

Since m/z = 127 overlaps with $C_{10}H_7$ and I atom, in order to further investigate this pinhole reaction separately on $C_{10}H_7$ and I atom, additional control experiments have been carried out using different precursors without acetylene: vinyliodide (C_2H_3I) and 1-bromonaphthalene ($C_{10}H_7Br$). As you can see from the Figure S3c, the result is consistent with H-addition reaction at short reaction times which we attribute to pinhole reaction. The m/z = 128 signal rapidly peaks at early time scale soon followed by decrease after the photolysis of 1-bromonaphthalene without acetylene. This result indicates that $C_{10}H_8$ is rapidly being formed through H-atom addition to 1-naphthalenyl radical likely due to pinhole reaction at the earliest times when the $C_{10}H_7$ radical concentration is high, but decreases at longer time scale as the concentration of $C_{10}H_7$ radicals drops due to recombination. In the case of the photolysis of vinyliodide without acetylene, m/z = 128 signal behavior contrasts with that when using 1-bromonaphthalene as a precursor: gradually increases with time with no initial peak, although a slight jump of m/z = 128 signal was observed around 400 us, likely due to pinhole reaction. But in case of I atom (m/z = 127), the wall reaction inside the reactor seems more dominant compared to pinhole reaction. This can be rationalized by relatively less reactive characteristic of I atom compared to naphthalenyl radical. If we simply apply linear combination between red open symbols and cyan open symbols from Figure S3c, we can qualitatively get the similar m/z = 128 behavior when using iodonaphthalene as a precursor shown in Figure S3d.

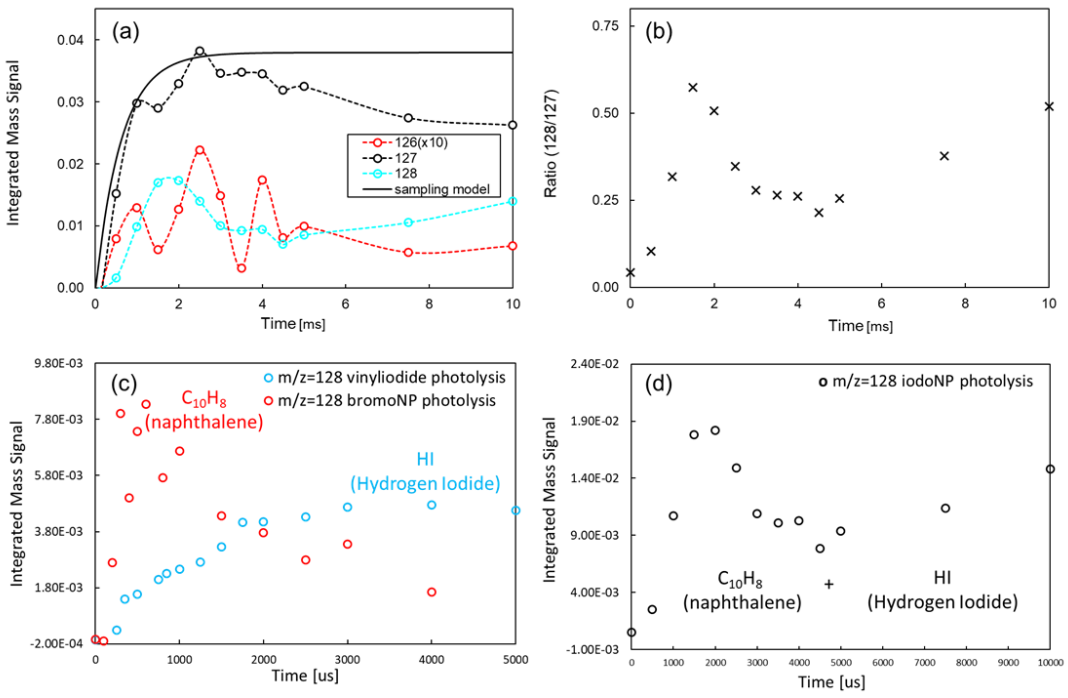

Figure S 3: (a) The comparison between time-dependent integrated mass spectral signals at m/z = 126, 127 and 128 measured up to 10 ms after the photolysis of 2-iodonaphthalene without acetylene at 700 K, 25 Torr. Open symbols (red: m/z = 126; black: m/z = 127; cyan: m/z = 128) indicate the signal from the experiments. Black solid line is the first order sampling rate model. (k_{sampling}= 1600 s^{-1}) (b) the ratio of integrated mass-spec signal at m/z = 128 to 127 up to 10 ms. (c) Time-dependent integrated mass spectral signals at m/z = 128 measured up to 5 ms after the photolysis of different precursors without acetylene under different experimental conditions. Red open symbols indicate the m/z = 128 signals observed after the photolysis of 1-bromonaphthalene at 300 K, 10 Torr. Cyan open symbols indicate the m/z = 128 signals observed after the photolysis of vinyliodide at 300 K, 25 Torr (d) Time-dependent integrated mass spectral signals at m/z = 128 measured up to 10 ms after the photolysis of 2-iodonaphthalene without acetylene at 700 K, 25 Torr.

3. SI related to KINETIC MODELING

3.1. A list of the estimated reactions in the kinetic model

In order to make reasonable estimated rates, a few reaction rates from previous references have been adopted to compare with the estimated rates. In the case of the recombination reaction $C_2H_3 + I \rightarrow C_2H_3I$, the vinyl radical self-reaction rate[3] has been set as the upper bound for this rate coefficient since I atom is less reactive than vinyl radical. C_2H_3 + N1-2 $\rightarrow$ VNP-2 has been calculated at the level of theory of CBS-QB3 using Transition State Theory. In the case of disproportionate reactions (e.g. N2-2 + I $\rightarrow$ ETN-2 + HI), the rates are estimated to be comparable to the rate of the reaction $C_2H_3 + Cl \rightarrow C_2H_2 + HCl$.[4]

Table S 1: Estimated Arrhenius equation parameters included in this study See Scheme 2 for definition of species labels.

Reactions	A	n	E_a (kcal mol^{-1})
C_2H_3 + N1-1 $\longrightarrow$ VNP−1	2.2×10^2	3.01	-8.251
C_2H_3 + N1-2 $\longrightarrow$ VNP−2	2.2×10^2	3.01	-8.251
$C_2H_3 + I \longrightarrow C_2H_3I$	1×10^{13}		
n-C_4H_5 + I $\longrightarrow$ C_4H_5I	1×10^{13}		
c-C_4H_5 + I $\longrightarrow$ C_4H_5I	1×10^{13}		
N1-1 + I $\longrightarrow$ $C_{10}H_7I$	1×10^{13}		
N1-2 + I $\longrightarrow$ $C_{10}H_7I$	1×10^{13}		
N2-2 + I $\longrightarrow$ $C_{12}H_9I$	1×10^{13}		
N2-1 + I $\longrightarrow$ $C_{12}H_9I$	1×10^{13}		
N17-2 + I $\longrightarrow$ $C_{12}H_9I$	1×10^{13}		
N6-2 + I $\longrightarrow$ $C_{12}H_9I$	1×10^{13}		
N11-1 + I $\longrightarrow$ $C_{12}H_9I$	1×10^{13}		
N11-2 + I $\longrightarrow$ $C_{12}H_9I$	1×10^{13}		
N7-1 + I $\longrightarrow$ $C_{12}H_9I$	1×10^{13}		
N7-2 + I $\longrightarrow$ $C_{12}H_9I$	1×10^{13}		
N6-1 + I $\longrightarrow$ $C_{12}H_9I$	1×10^{13}		
N8-2 + I $\longrightarrow$ $C_{12}H_9I$	1×10^{13}		
N14-2 + I $\longrightarrow$ $C_{12}H_9I$	1×10^{13}		
N14-1 + I $\longrightarrow$ $C_{12}H_9I$	1×10^{13}		
AN1 + I $\longrightarrow$ $C_{12}H_9I$	1×10^{13}		
AN2 + I $\longrightarrow$ $C_{12}H_9I$	1×10^{13}		
N8-1 + I $\longrightarrow$ $C_{12}H_9I$	1×10^{13}		
N16-2 + I $\longrightarrow$ $C_{12}H_9I$	1×10^{13}		

Reactions	A	n	E_a (kcal mol^{-1})
$C_2H_3 + I \longrightarrow C_2H_2 + HI$	5.7×10^6	2.70	0.956
n-C_4H_5 + I $\longrightarrow$ C_4H_4 + HI	5.7×10^6	2.70	0.956
c-C_4H_5 + I $\longrightarrow$ C_4H_4 + HI	5.7×10^6	2.70	0.956
N2-2 + I $\longrightarrow$ ETN-2 + HI	5.7×10^6	2.70	0.956
N2-1 + I $\longrightarrow$ ETN-1 + HI	5.7×10^6	2.70	0.956
N17-2 + I $\longrightarrow$ CBaN[a] + HI	5.7×10^6	2.70	0.956
N6-2 + I $\longrightarrow$ CBaN + HI	5.7×10^6	2.70	0.956
N11-2 + I $\longrightarrow$ CBbN[b] + HI	5.7×10^6	2.70	0.956
N11-1 + I $\longrightarrow$ CBaN + HI	5.7×10^6	2.70	0.956
N7-2 + I $\longrightarrow$ CBbN + HI	5.7×10^6	2.70	0.956
N7-1 + I $\longrightarrow$ CBaN + HI	5.7×10^6	2.70	0.956
N6-1 + I $\longrightarrow$ CBaN + HI	5.7×10^6	2.70	0.956
N8-2 + I $\longrightarrow$ CBaN + HI	5.7×10^6	2.70	0.956
N14-2 + I $\longrightarrow$ ETN-2 + HI	5.7×10^6	2.70	0.956
N14-1 + I $\longrightarrow$ CBaN + HI	5.7×10^6	2.70	0.956
AN1 + I $\longrightarrow$ ACN + HI	5.7×10^6	2.70	0.956
AN2 + I $\longrightarrow$ ACN + HI	5.7×10^6	2.70	0.956
N8-1 + I $\longrightarrow$ ACN + HI	5.7×10^6	2.70	0.956
N16-2 + I $\longrightarrow$ CBbN + HI	5.7×10^6	2.70	0.956

[a,b] $C_{12}H_8$ isomer. Negligible amount was formed in the model prediction.

3.2. A list of the additional PICS info

Table S 2: Supplementary Photoionization cross-sections (PICS)

m/z	Species	PICS (Mb)	2 σ Uncertainty (Mb)	Reference
52	vinylacetylene	32	± 2	Ref. 5
68	furan	14	± 3	Ref. 6
78	benzene	30	± 4	Ref. 7
78	fulvene	30	± 4	[a]
84	cyclohexane	20	± 4	Ref. 5
92	toluene	31	± 3	Ref. 8
100	n-heptane	10	± 1	Ref. 8
127	I	74	+33 -23	Ref. 9
128	HI	80	± 40[b]	Ref. 10

[a] assumed to have the same PICS of benzene

[b] assumed with a 50% uncertainty

3.3. Estimation of initial concentration of $C_{10}H_7$ radical determined from the observed signal at m/z=127

The first-order sampling rate method was also used to determine the initial concentration of $C_{10}H_7$ radical, $[C_{10}H_7]_0$ as shown in Figure S4. It was assumed in the model that the initial concentration of the I atom determined from the observed signal at m/z=127 was equal to $[C_{10}H_7]_0$. This assumption is reasonable since the kinetic modeling showed that most $C_{10}H_7$ radicals were consumed before I atom reached its peak (within 2 ms), and the PICS of I atom (74 Mb) is expected to be significantly larger than that of $C_{10}H_7$ (13 Mb; assumed to be same as the PICS of vinyl radical). [9, 11]

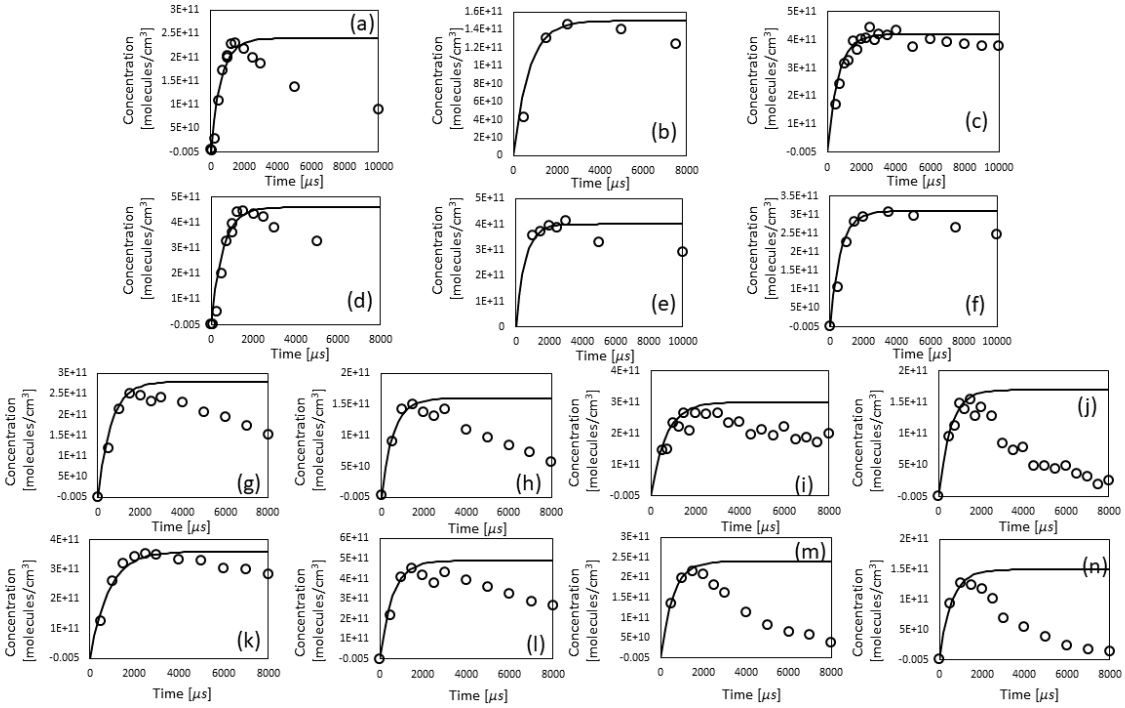

Figure S 4: The first-order sampling rate method used to determine the initial concentration of $C_{10}H_7$ radical, $[C_{10}H_7]_0$, in the model assuming that the initial concentration of the I atom determined from the observed signal at m/z=127 is equal to $[C_{10}H_7]_0$. Reactor conditions were (a) 1-naphthalenyl + C_2H_2, 500 K, 25 Torr; (b) 1-naphthalenyl + C_2H_2, 700 K, 25 Torr; (c) 1-naphthalenyl + C_2H_2, 800 K, 25 Torr; (d) 1-naphthalenyl + C_2H_2, 500 K, 50 Torr; (e) 1-naphthalenyl + C_2H_2, 700 K, 50 Torr; (f) 1-naphthalenyl + C_2H_2, 800 K, 50 Torr; (g) 2-naphthalenyl + C_2H_2, 500 K, 15 Torr; (h) 2-naphthalenyl + C_2H_2, 600 K, 15 Torr; (i) 2-naphthalenyl + C_2H_2, 700 K, 15 Torr; (j) 2-naphthalenyl + C_2H_2, 800 K, 15 Torr; (k) 2-naphthalenyl + C_2H_2, 500 K, 25 Torr; (l) 2-naphthalenyl + C_2H_2, 600 K, 25 Torr; (m) 2-naphthalenyl + C_2H_2, 700 K, 25 Torr; (n) 2-naphthalenyl + C_2H_2, 800 K, 25 Torr. Black open circles indicate the signal at m/z = 127; Black solid line is the first order sampling rate model.

4. SI related to RESULTS AND DISCUSSION

4.1. Pressure dependence of 2-naphthalenyl + C_2H_2 system

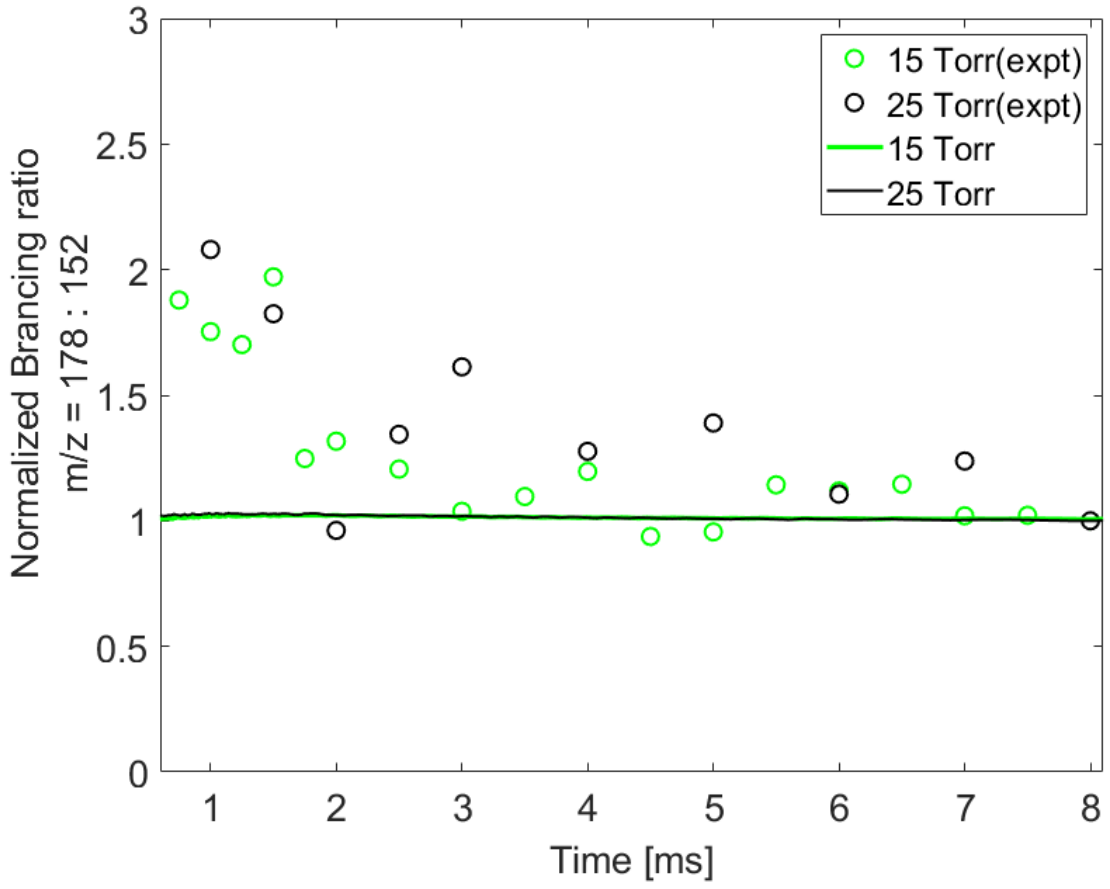

Figure S 5: The normalized branching ratio of m/z = 178 to m/z = 152 in 2-naphthalenyl + C_2H_2 at various time delays. The experimentally observed and the model simulated branching ratio values at various time were normalized to corresponding value at 8 ms. Open circle symbols indicate the experimentally observed ratio of m/z = 178 to m/z = 152 under each experimental condition (green: 800 K, 15 Torr, and black: 800 K, 25 Torr); Solid lines indicate model predicted ratio of m/z = 178 to m/z = 152 under each experimental condition (green: 800 K, 15 Torr, and black: 800 K, 25 Torr).

4.2. Additional Experimental Data

In this section, we provide additional experimental data that was not included in the main manuscript but discussed below.

4.2.1. Discussion on the side products

As shown in Figure S7 and S11 the model captured all these side products (i.e. m/z = 127: I atom; m/z = 128: HI atom; m/z = 52, vinylacetylene (C_4H_4); m/z = 78: benzene and fulvene). According to

the model prediction, vinylacetylene, benzene, and fulvene production originated from acetylene addition to vinyl radical (formed from the side reaction C_2H_2+H). The side chemistry model significantly overpredicted vinylacetylene (m/z = 52) production, but this turned out to be less sensitive on the model chemistry of interest (i.e. acetylene addition to naphthaleneyl radical). The overprediction might indicate incorrect other estimated side reactions affecting C_4H_4 formation (e.g. C_4H_3I formation chemistry). Although these behaviors might be interesting for future studies, C_4H_4 chemistry was beyond the scope of the current work. It is observed that the m/z = 127 signal decreased after 2 ms, primarily reflecting I atom consumption; this behavior shows a negative temperature dependence between 500 K and 800 K in 1-naphthalenyl + C_2H_2 system, while I atom consumption showed positive temperature dependence in 2-naphthalenyl + C_2H_2 system. All these discrepancies indicate that adopted or estimated I atom chemistry in the model might not be precise enough to explain I atom consumption throughout the whole experimental conditions. I atom consumption was beyond the scope of the current work to investigate the PAHs formation from naphthalenyl + acetylene, although this reaction might be interesting for future studies.

4.2.2. Discussion on discrepancy of m/z = 153 signals for more experimental conditions

In Figure S8a and S10a (both 500 K), the model predicted m/z = 153 signal is mostly attributed to $C_{12}H_9$ non-RSR species, so we can see huge discrepancy between the observed m/z = 153 signal and model prediction. In Figure S8b and S10b (both 600 K), the model predicted m/z = 153 signal is also mostly attributed to $C_{12}H_9$ non-RSR species, so we can claim that the discrepancy before 4 ms is due to unusually small PICS of $C_{12}H_9$ non-RSR species. However, after 4 ms, the model agreement with the experimental data is good. which is not consistent with the hypothesis mentioned. We don't understand this behavior. In Figure S8c and S10c (both 700 K), the model agreement is good after 3 ms. This is because m/z = 153 signal after 3 ms is mostly attributed to $C_{12}H_9$ RSR species isomerized from $C_{12}H_9$ non-RSR species. In Figure S8d and S10d (both 800 K), the model agreement is within the uncertainty ranges. This is because at high temperature, $C_{12}H_9$ RSR species become dominant in the system.

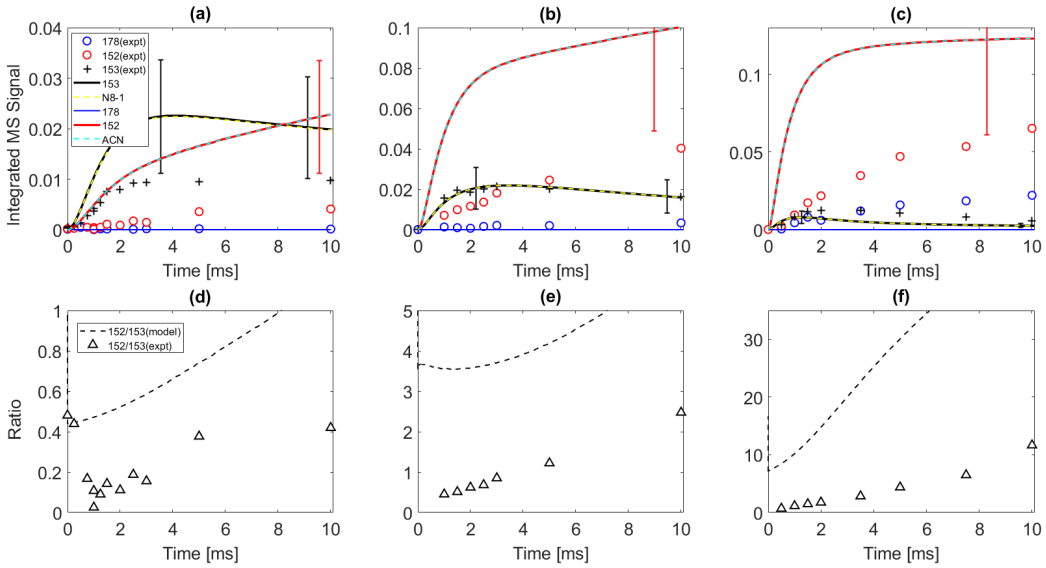

Figure S 6: (top) Time-dependent integrated m/z signals measured up to 10 ms after the photolysis of the 1-iodonaphthalene in the presence of C_2H_2. Red open circles indicate the m/z=152 signal; blue open circles indicate m/z=178 signal; and the black cross symbols (+) indicate the m/z=153 signal from the experiment. Solid lines (red: m/z=152, blue: m/z=178, and black: m/z=153); and dashed lines (yellow: N8-1; cyan: ACN, acenaphthylene) correspond to the model prediction under each set of experimental conditions. In (c), the black solid line (including its error bars), yellow dashed line, and black cross symbols have been multiplied by 8 for scale. Uncertainty ranges of the model predictions (due to uncertainties in PICS) are shown as error bars. (Bottom) The branching ratio of m/z=152 to m/z=153. Black open triangle symbols indicate the experimentally observed ratio of m/z=152 to m/z=153; Black dashed line indicates model predicted ratio of m/z=152 to m/z=153. Reactor conditions: (a) and (d) 500 K, 50 Torr, initial radical concentration $[C_{10}H_7]_0 = 4.6 \times 10^{11}$ molecules cm^{-3}; (b) and (e) 700 K, 50 Torr, $[C_{10}H_7]_0 = 4.0 \times 10^{11}$ molecules cm^{-3}; (c) and (f) 800 K, 50 Torr, $[C_{10}H_7]_0 = 3.1 \times 10^{11}$ molecules cm^{-3}. The concentration of C_2H_2 for all the experiments was 3×10^{16} molecules/cm^3.

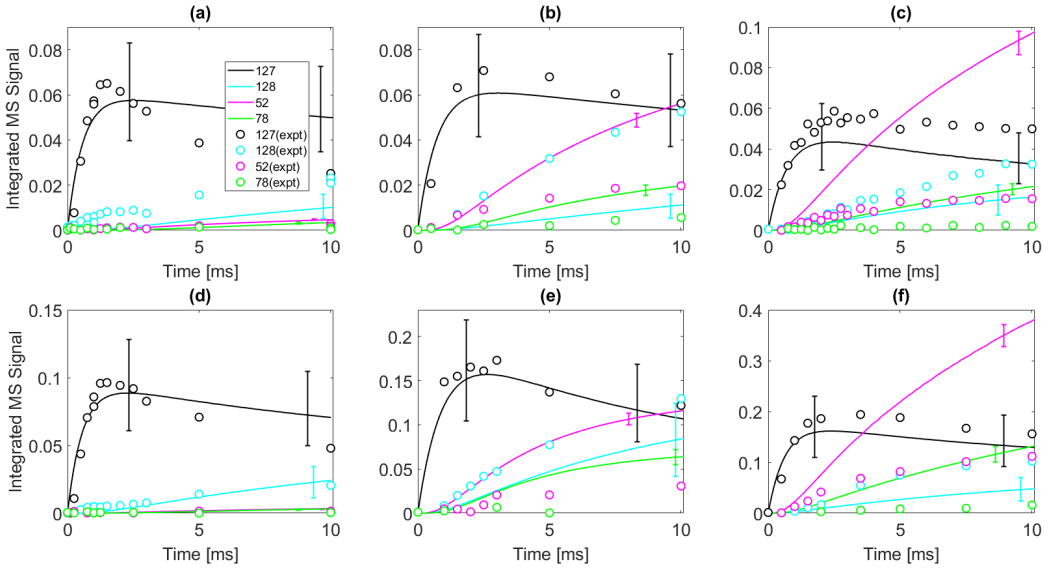

Figure S 7: The comparison between time-dependent integrated mass spectral signals at m/z = 52, 78, 127, and 128 and the model prediction of corresponding mass channel under various experimental conditions. Open symbols (black: m/z = 127; cyan: m/z = 128; magenta: m/z = 52, green: m/z = 78) indicate the signal from the experiments and solid lines correspond to the model prediction under each condition. Uncertainty ranges of the model predictions (due to uncertainties in PICS) are shown as error bars. Reactor conditions were (a) 500 K, 25 Torr; (b) 700 K, 25 Torr; (c) 800 K, 25 Torr; (d) 500 K, 50 Torr; (e) 700 K, 50 Torr; (f) 800 K, 50 Torr.

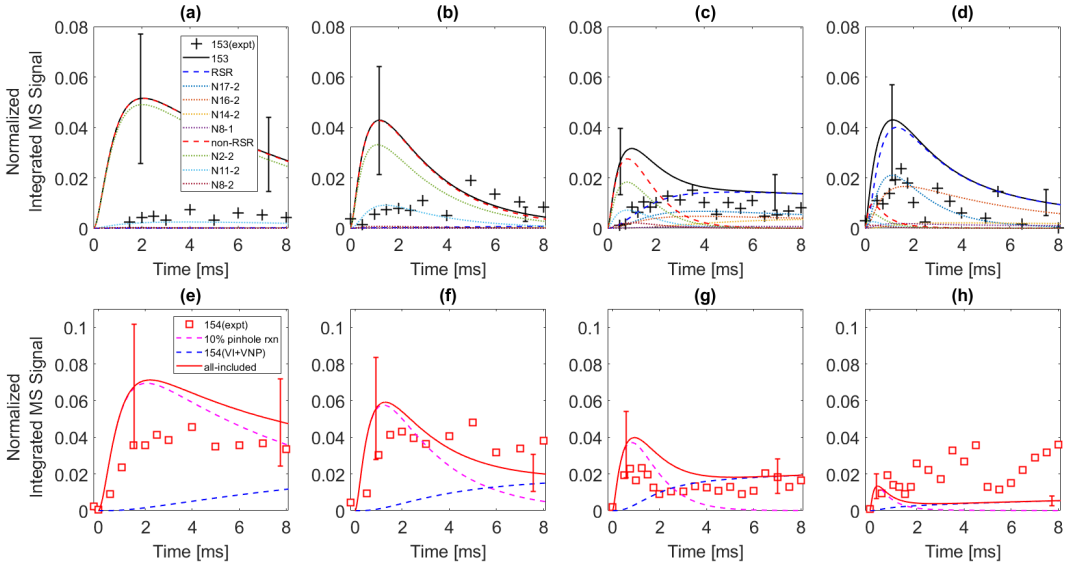

Figure S 8: (Top) The comparison between time-dependent integrated mass spectral signals at m/z=153 measured up to 8 ms after the photolysis pulse for the reaction of 2-naphthalenyl radical with C_2H_2 under various experimental conditions and the model prediction of m/z=153 products which are radical species (both RSR and non-RSR). Black cross symbols indicate the signal at m/z=153; solid black line is a sum of red dashed line ($C_{12}H_9$ non-RSR species) and blue dashed line ($C_{12}H_9$ RSR species) that indicate the model prediction under various experimental conditions. Dotted lines indicate each labeled $C_{12}H_9$ radical species. The notation in the legends is described in Scheme 2. (Bottom) The comparison between time-dependent integrated mass spectral signals at m/z=154 and the model prediction of corresponding mass channel under various experimental conditions. Red open square symbols indicate the signal at m/z=154 from the experiments. Dashed lines (magenta: vinylnaphthalene originated from H-atom addition to 10% of each $C_{12}H_9$ non-RSR species at the pinhole; blue: vinyliodide + vinylnaphthalene formed through $C_{12}H_9$ + H atom from secondary chemistry), and red solid line (sum of all dashed lines) correspond to the model prediction under each condition. Uncertainty ranges of the model predictions (due to uncertainties in PICS) are shown as error bars. Reactor conditions were (a) and (e) 500 K, 15 Torr; (b) and (f) 600 K, 15 Torr; (c) and (g) 700 K, 15 Torr; (d) and (h) 800 K, 15 Torr

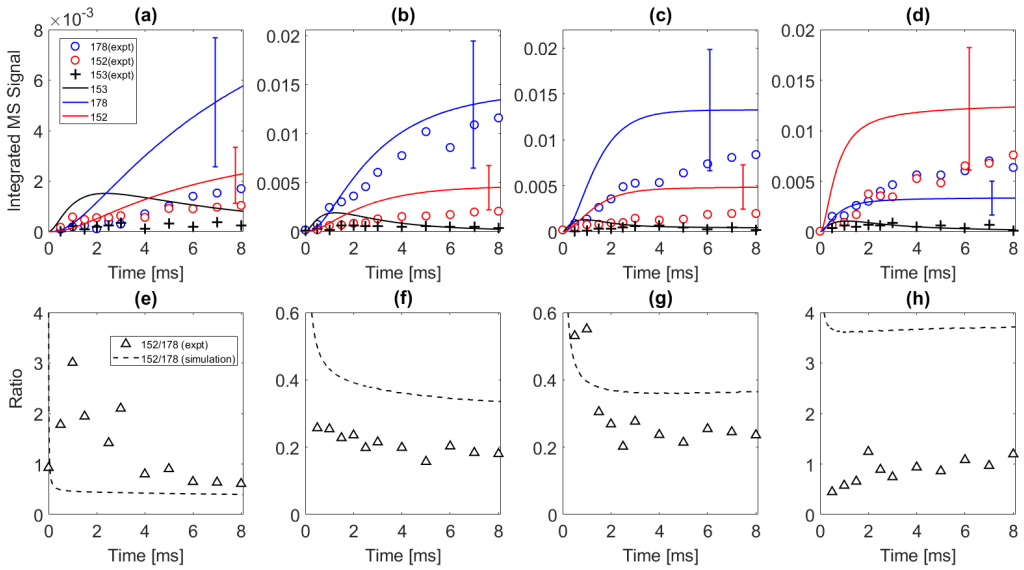

Figure S 9: (top) Time-dependent species concentrations measured up to 8 ms after the photolysis pulse for the reaction of 2-naphthalenyl radical with acetylene. Red open circles indicate the signal at m/z=152; blue open circles indicate the signal at m/z=178; black crosses indicate the signal at m/z=153. Solid lines correspond to the model prediction under each experimental condition: red solid line indicates m/z=152; blue solid line indicates m/z=178; black solid line indicates m/z=153 species. Uncertainty ranges of the model predictions (due to uncertainties in PICS) are shown as error bars. (bottom) The product branching ratio between m/z=152 and m/z=178. Black open triangle symbols indicate the experimentally observed ratio of m/z=152 to m/z=178; Black dashed line indicates predicted ratio of m/z=152 to m/z=178 from the model simulation. Reactor conditions were (a) and (e) 500 K, 25 Torr, initial radical concentration $[C_{10}H_7]_0 = 3.6 \times 10^{11}$ molecules cm^{-3}; (b) and (f) 600 K, 25 Torr, initial radical concentration $[C_{10}H_7]_0 = 4.9 \times 10^{11}$ molecules cm^{-3}; (c) and (g) 700 K, 25 Torr, initial radical concentration $[C_{10}H_7]_0 = 3.1 \times 10^{11}$ molecules cm^{-3}; (d) and (h) 800 K, 25 Torr, initial radical concentration $[C_{10}H_7]_0 = 2.1 \times 10^{11}$ molecules cm^{-3}. The concentration of C_2H_2 for all the experiments was 3×10^{16} molecules/cm^3.

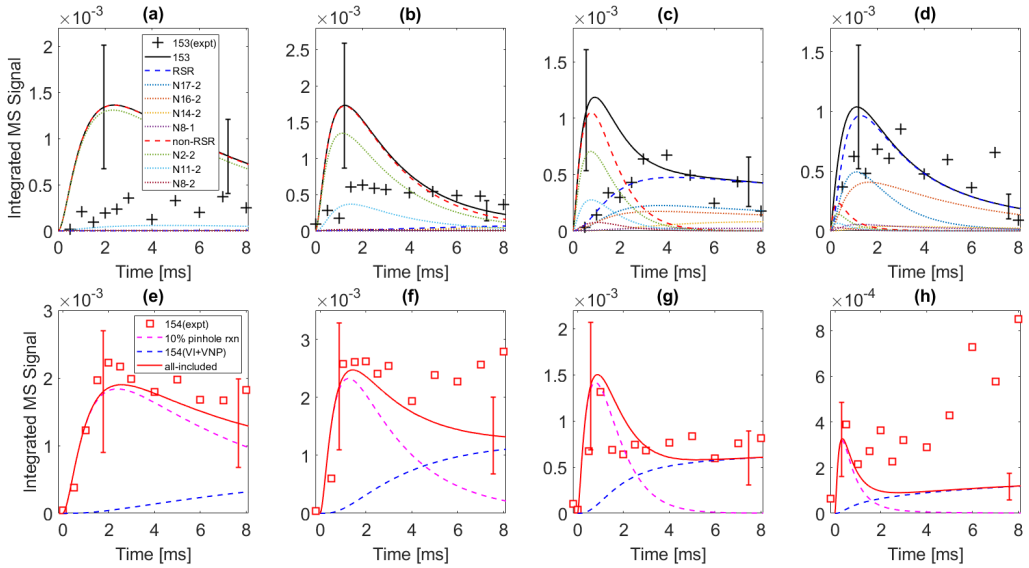

Figure S 10: (Top) The comparison between time-dependent integrated mass spectral signals at m/z=153 measured up to 8 ms after the photolysis pulse for the reaction of 2-naphthalenyl radical with C_2H_2 under various experimental conditions and the model prediction of m/z=153 products which are radical species (both RSR and non-RSR). Black cross symbols indicate the signal at m/z=153; solid black line is a sum of red dashed line ($C_{12}H_9$ non-RSR species) and blue dashed line ($C_{12}H_9$ RSR species) that indicate the model prediction under various experimental conditions. Dotted lines indicate each labeled $C_{12}H_9$ radical species. The notation in the legends is described in Scheme 2. (Bottom) The comparison between time-dependent integrated mass spectral signals at m/z=154 and the model prediction of corresponding mass channel under various experimental conditions. Red open square symbols indicate the signal at m/z=154 from the experiments. Dashed lines (magenta: vinylnaphthalene originated from H-atom addition to 10% of each $C_{12}H_9$ non-RSR species at the pinhole; blue: vinyliodide + vinylnaphthalene formed through $C_{12}H_9$ + H atom from secondary chemistry), and red solid line (sum of all dashed lines) correspond to the model prediction under each condition. Uncertainty ranges of the model predictions (due to uncertainties in PICS) are shown as error bars. Reactor conditions were (a) and (e) 500 K, 25 Torr; (b) and (f) 600 K, 25 Torr; (c) and (g) 700 K, 25 Torr; (d) and (h) 800 K, 25 Torr

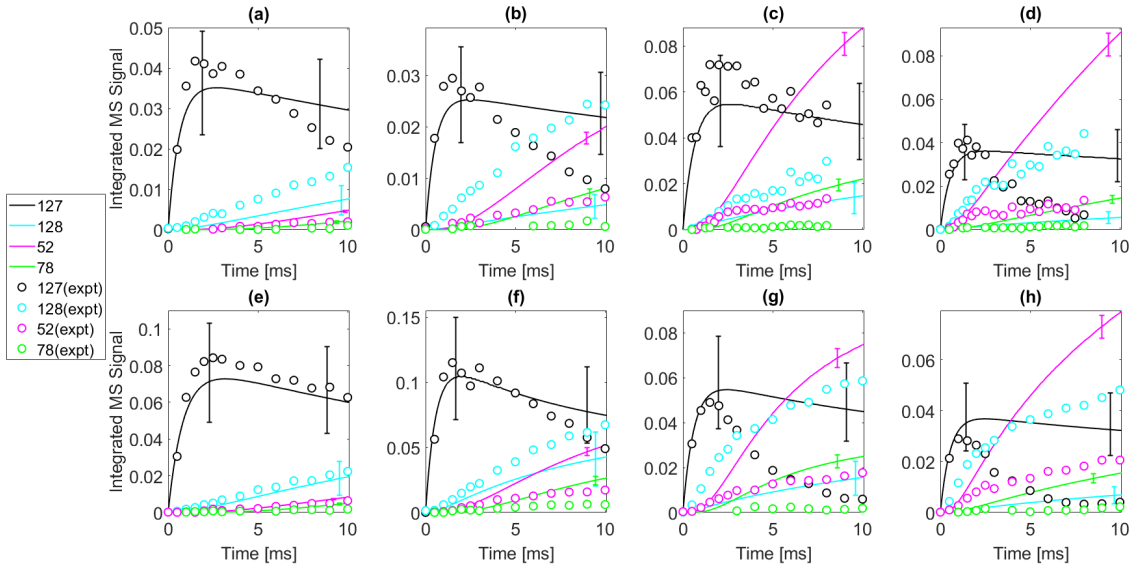

Figure S 11: The comparison between time-dependent integrated mass spectral signals at m/z = 52, 78, 127, and 128 and the model prediction for corresponding mass under various experimental conditions. Open symbols (black: m/z = 127; cyan: m/z = 128; magenta: m/z = 52, green: m/z = 78) indicate the signal from the experiments and solid lines correspond to the model prediction under each condition. Reactor conditions were (a) 500 K, 15 Torr; (b) 600 K, 15 Torr; (c) 700 K, 15 Torr; (d) 800 K, 15 Torr; (e) 500 K, 25 Torr; (f) 600 K, 25 Torr; (g) 700 K, 25 Torr; (h) 800 K, 25 Torr.

4.3. Rate of Production Analysis

In this section, the ROP analysis data are available

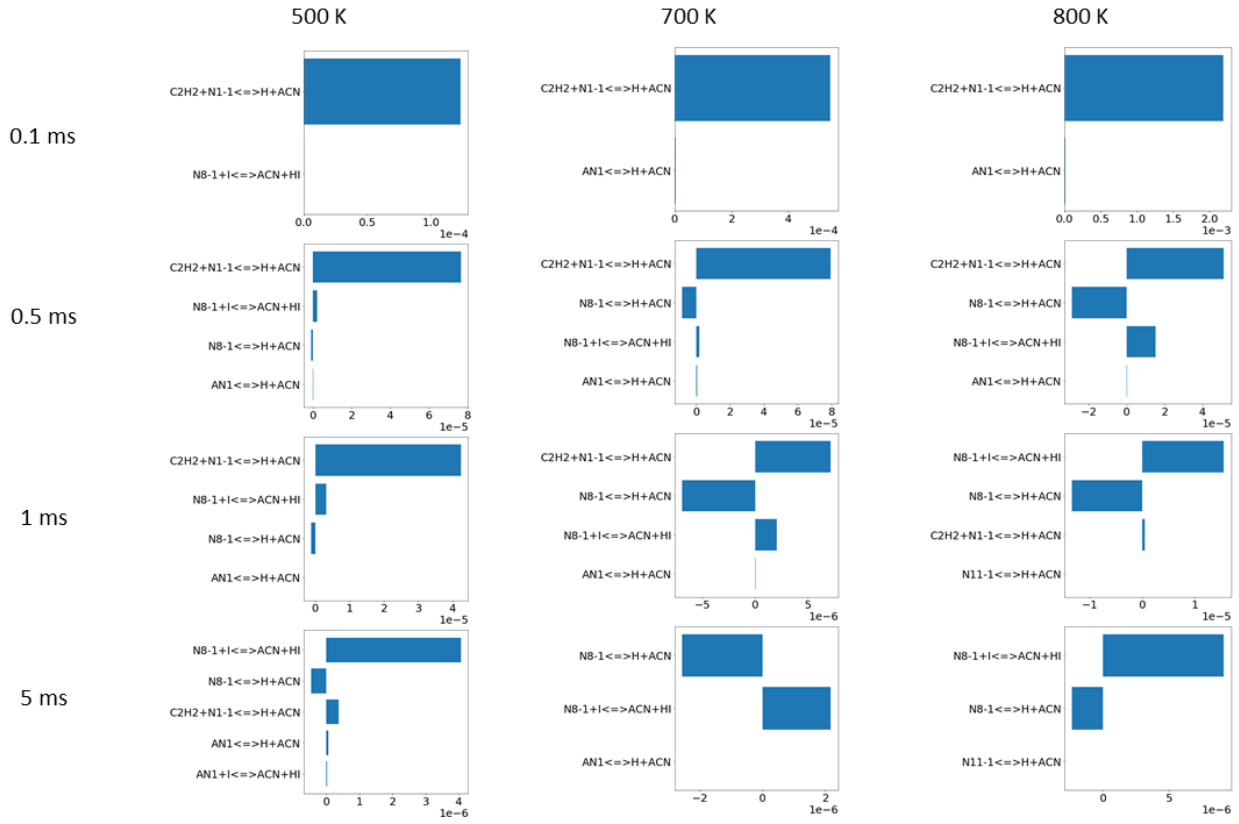

Figure S 12: Rate of production analysis on acenaphthylene in 1-naphthalenyl + C_2H_2 system. Each row represents corresponding time and each column represents corresponding temperature

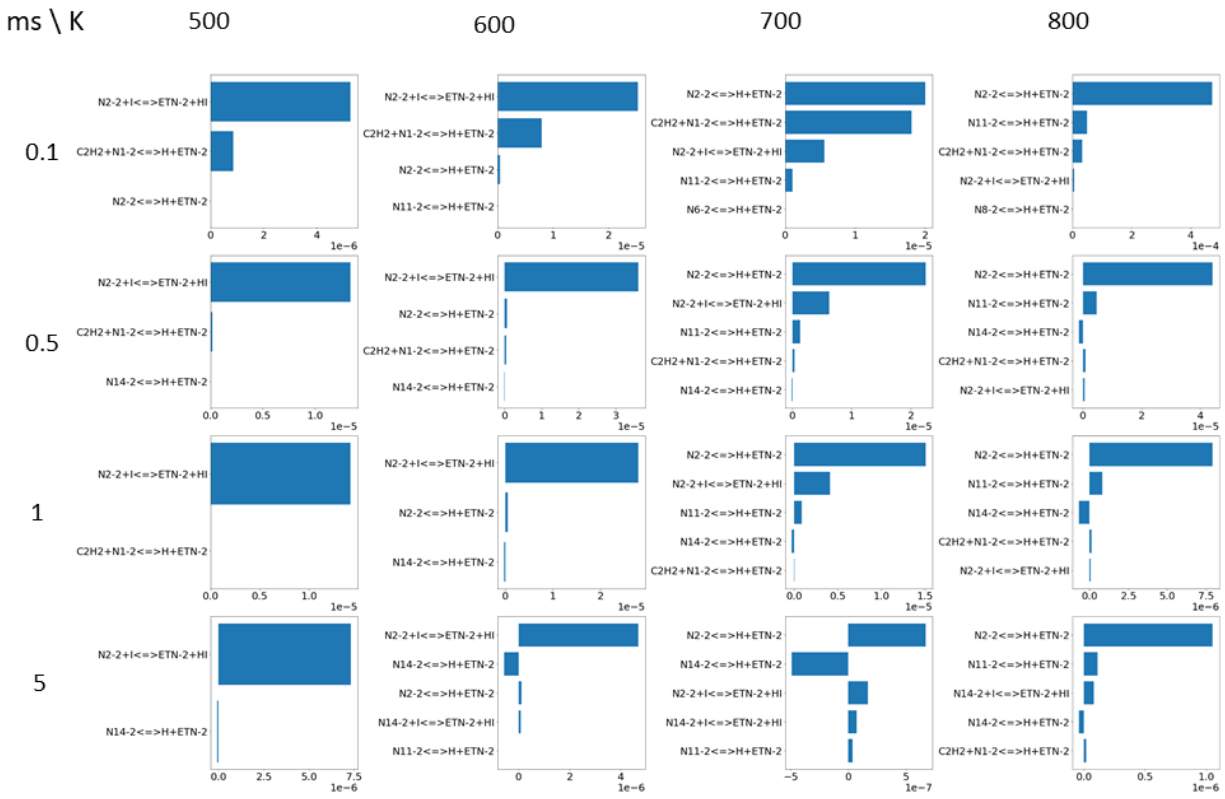

Figure S 13: Rate of production analysis on 2-ethynylnaphthalene in 2-naphthalenyl + C_2H_2 system. Each row represents corresponding time and each column represents corresponding temperature

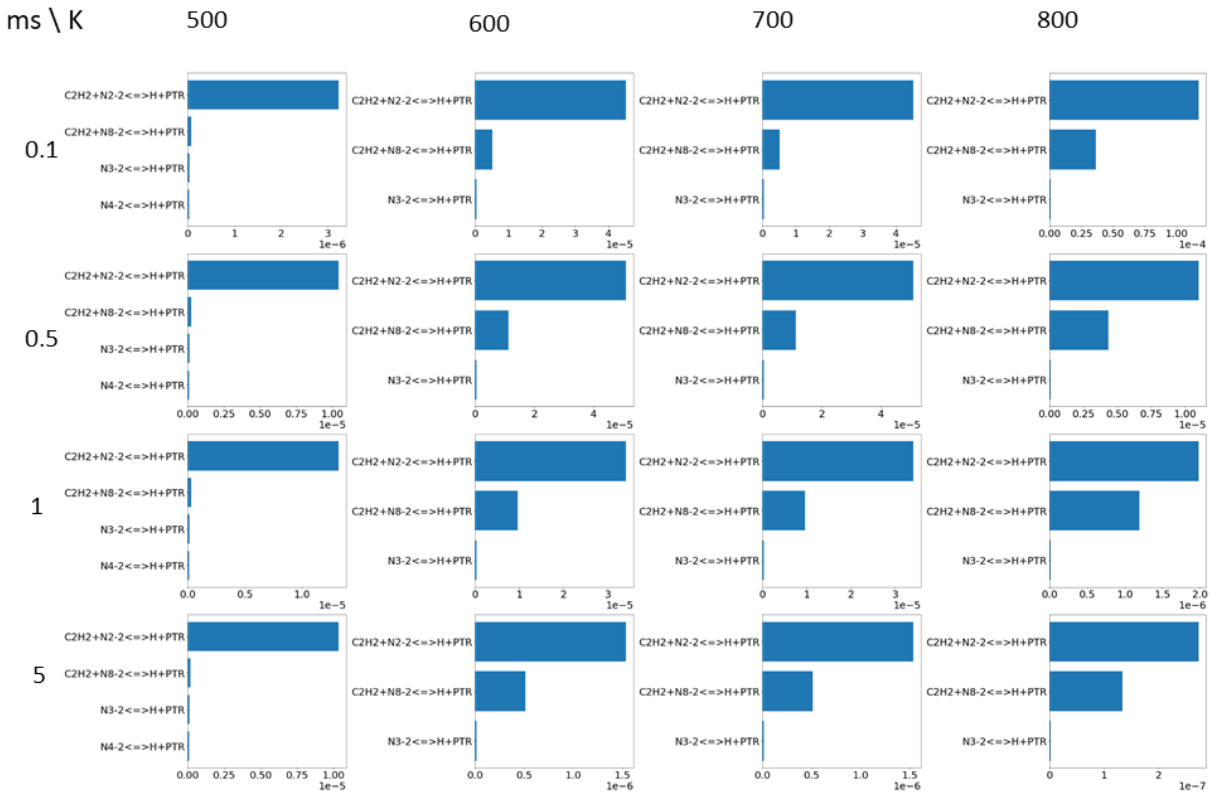

Figure S 14: Rate of production analysis on phenanthrene in 2-naphthalenyl + C_2H_2 system. Each row represents corresponding time and each column represents corresponding temperature

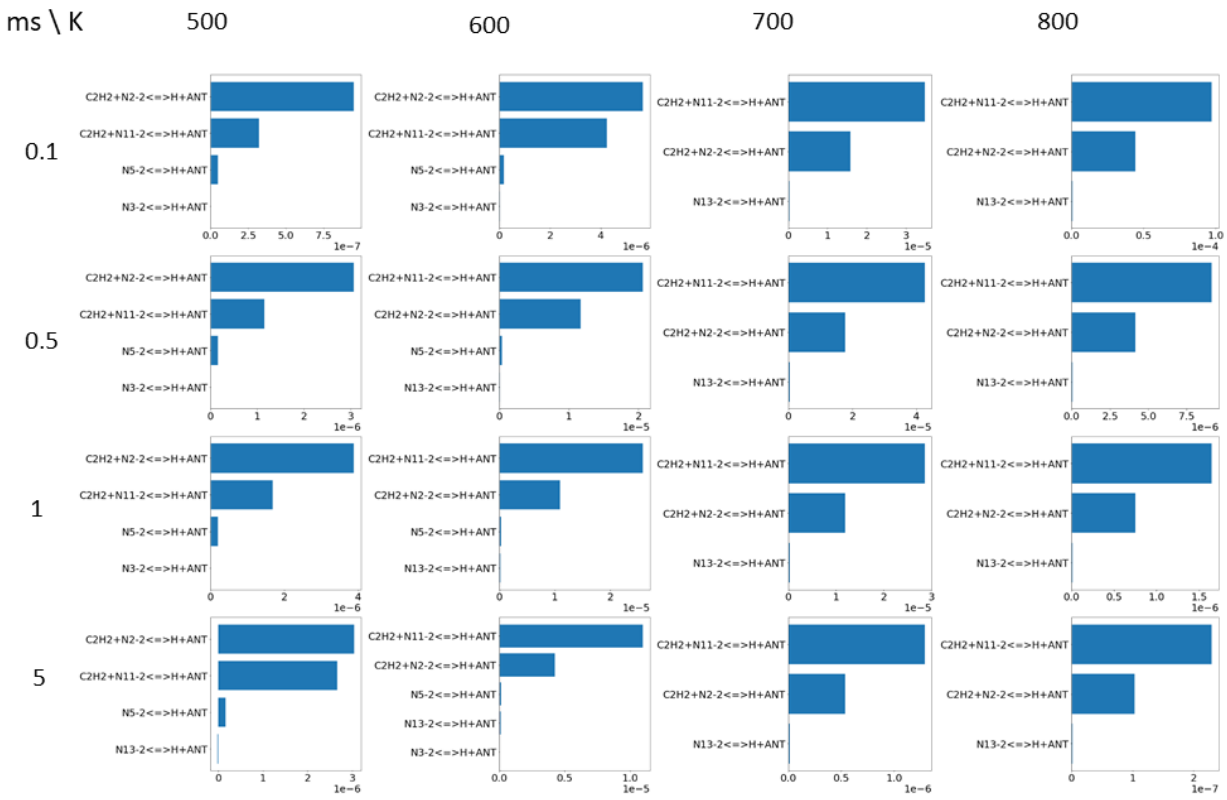

Figure S 15: Rate of production analysis on anthracene in 2-naphthalenyl + C_2H_2 system. Each row represents corresponding time and each column represents corresponding temperature

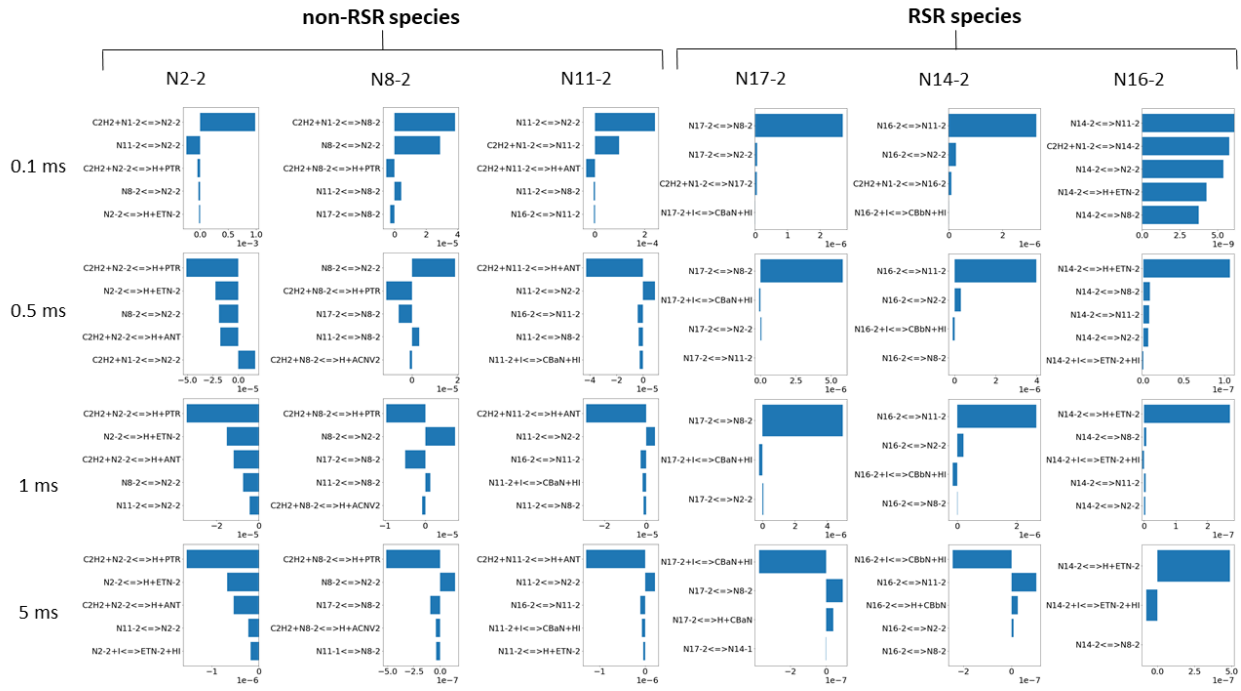

Figure S 16: Rate of production analysis on major $C_{12}H_9$ species (N2-2, N8-2, N11-2, N17-2, N14-2, and N16-2) in 2-naphthalenyl + C_2H_2 system at 700 K and 15 Torr. Each row represents corresponding time and each column represents corresponding species in order

4.4. Model simulation with reduced PICS of Acenaphthylene (ACN)

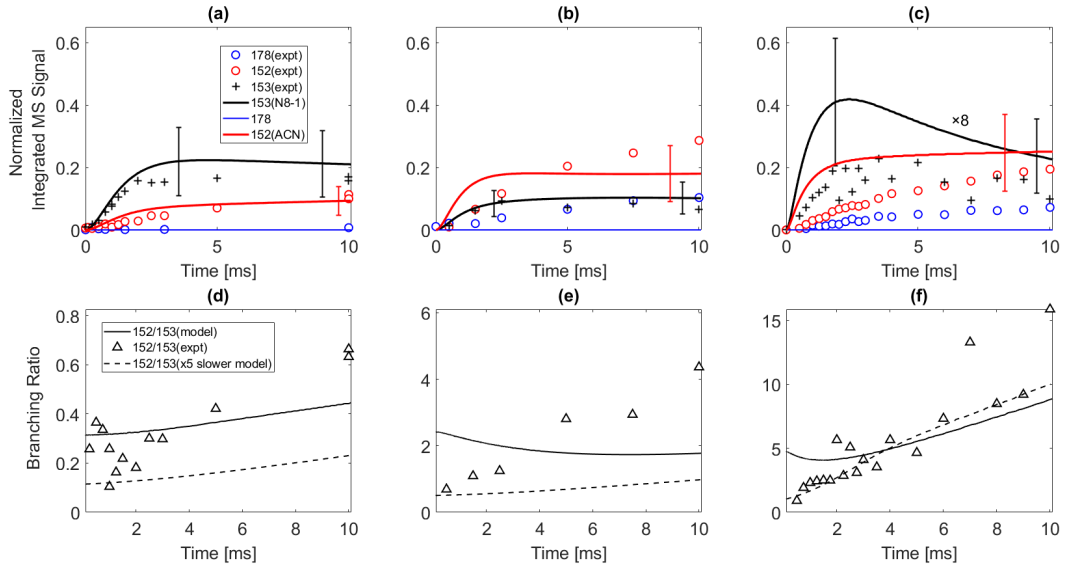

Figure S 17: Corresponding to Figure 2 in the main text. The only difference is that the PICS of ACN has been reduced by a factor of three (54 Mb → 18 Mb)

4.5. Discrepancy (ii): Unexpected observation on m/z = 178 signal in 1-iodonaphthalene experiments

Discrepancy (ii) is the unexpected appearance of m/z = 178 signal when 1-naphthalenyl is reacted with C_2H_2 at temperatures ≥700 K as can be observed in Figure 2. Although m/z = 178 species such as phenanthrene and anthracene are predicted (and observed) to be major products from 2-naphthalenyl, none of the theoretical studies predict significant m/z =178 formation from 1-naphthalenyl. We consider many potential explanations for this discrepancy: (ii.1) impurity in starting material, (ii.2) fast isomerization of the nascent radicals, (ii.3) a missing C_2H_2 addition reaction in the mechanism, (ii.4) secondary chemistry of C_2H_3 side product forms m/z=178, (ii.5) significant misestimation of rate coefficients for reactions in the model, and (ii.6) much of the m/z = 178 observed is C_4H_3I rather than $C_{14}H_{10}$. Each is discussed in turn here. First, we consider the possibility of opposing isomer contamination (2-iodonaphthalene) in the precursor (1-iodonaphthalene), explanation (ii.1). If 2-iodonaphthalene were present in the reactor during the 1-iodonaphthalene experiments, then some 2-naphthalenyl radical would be formed, and that would form C_{14} PAHs through sequential acetylene addition. However, as mentioned in the experimental section, the opposing isomer contamination in the starting material has been measured to be less than 0.5% by NMR. It is possible that the 2-iodonaphthalene impurity level in the reactor is higher than in the starting material (e.g. if there was some 2-iodonaphthalene carry-over in the apparatus from earlier experiments, or if some of the 1-iodonaphthalene isomerizes to 2-naphthalene on the walls of the reactor.) However, even assuming 10% of 2-naphthalenyl radical included in initial naphthalenyl radical concentration under the experimental

condition same as Figure 2c, this could only explain up to 17% of m/z = 178 mass signal observed in Figure 2c. Extremely high contamination, which reproducibly varied in specific ways depending on the experimental conditions, would be required for isomer contamination to explain the data. This is implausible. So we don't believe isomer contamination can explain our observation of significant m/z=178 signal in the 1-naphthalenyl experiments.

We considered the possibility (ii.2) that the observed discrepancy may be due to improper treatment of the isomerization between 1-naphthalenyl and 2-naphthalenyl radicals. For example, excess energy deposition in 1-naphthalenyl radicals produced by the photolysis laser flash could cause isomerization to 2-naphthalenyl before the nascent radical is thermalized by the bath gas. To assess this possibility, a simple assessment of this isomerization was performed using Rice-Ramsperger-Kassel-Marcus (RRKM) theory [12] and the result suggested that isomerization was negligible at our experimental conditions. The detailed calculation is presented in the Supplementary Information 4.5.

We now consider hypothesis (ii.3), that another reaction pathway, previously not considered in the model chemistry [13] exists. The fact that species N8-1 was formed in significant amounts in the model under every temperature condition (Figures 2a–2c) suggests that its reaction with C_2H_2 might be important; however, the second C_2H_2 addition to N8-1 in Scheme 1 has not been considered in the model. This might suggest that another species formed by the second C_2H_2 addition to N8-1, not considered, may be responsible for the signal at m/z = 178. A set of CBS-QB3 ab initio calculations of the second acetylene reaction to N8-1 has been carried out using Automated Reaction Calculator (ARC) and Gaussian 16, and the new reaction with the lowest barrier is shown in Figure S18 in the Supplementary Information.[14, 15] However, the reaction (High-pressure limit rate coefficient $k = 5.99 \times 10^6\,\mathrm{cm^3\,mol^{-1}\,s^{-1}}$ at 800 K to form m/z = 179 that is followed by immediate dissociation to m/z = 178) was able to account for only 5% of observed m/z = 178. The level of theory used in the literature kinetic model was G3(MP2,CC) [13], while the level employed here was CBS-QB3, which is not quite as accurate. To test the sensitivity of the N8-1 + C_2H_2 reaction rate to possible errors in the computed barrier height, the rate coefficient of this reaction at 800 K was calculated with a 2 kcal/mol lower barrier height. This rate coefficient k was $1.26 \times 10^7\,\mathrm{cm^3\,mol^{-1}\,s^{-1}}$ at 800 K, which can only account for up to 15% of observed m/z = 178. So while the N8-1 +C_2H_2 reaction is not completely negligible, it does not appear to be fast enough to explain the large observed m/z=178 signal.

The bimolecular reaction between vinyl radical (C_2H_3) and N8-1 forming H radical and a product at m/z = 179 was also considered as a possible source of m/z = 178, hypothesis (ii.4). This reaction was added to the kinetic model with an intentionally overestimated rate of $k = 3.0 \times 10^{14}\,\mathrm{cm^3\,mol^{-1}\,s^{-1}}$ to assess its potential significance. However, this reaction only accounted for up to 11% of the observed m/z = 178 even assuming immediate and full dissociation of the species at m/z = 179 (from the bimolecular reaction above) into a stable product with m/z = 178 and H atom (see the red pathway in Figure S18 and the model prediction in Figure S 19c). So this reaction cannot explain the observations.

Another hypothesis (ii.5) for the discrepancy between model and experiment is that the parameters used

to describe the reaction kinetics and the thermochemistry in the model are inaccurate. If the well-skipping reaction of 1-naphthalenyl radical + C_2H_2 to form acenaphthylene is overpredicted in the model, the ratio of 152:153 predicted by the model at early times would be way off, and the concentration of 153 would be underpredicted, affecting the predictions of the rates of the subsequent reactions that convert 153 into 152 (and 178). To test this hypothesis, a sensitivity analysis under the experimental condition similar to Figure 2c was performed for each yield of phenanthrene, anthracene, and $C_{14}H_{10}$ (m/z = 178 species in Figure S18) to help identify reaction parameters the reactions are sensitive toward and determine if an improvement can be achieved by adjusting a certain parameter (See Figure S20). In Figure S20a and b, the computed k for the well-skipping reaction of 1-naphthalenyl radical + C_2H_2 to form acenaphthylene has the largest $\frac{d(lnC_n)}{d(k_i)}$ of around -1 on both phenanthrene and anthracene formation (where C_n is the concentration of the species n and k_i is the rate coefficient of the reaction i). So reducing this k for the well-skipping reaction by a factor of 5 will increase the yield of phenanthrene and anthracene by about 5 times (if we assume the sensitivity coefficient is constant with respect to well-skipping reaction rate coefficient k). This might suggest that adjustment in other rate coefficients can improve the agreement between the model and the experimental data further. However, it has to be noted that the the model prediction on m/z = 178 signal is about 4 orders of magnitude smaller than experimentally observed signal at m/z = 178. We do not believe the values of the rate coefficients in the model, which are derived from quantum chemistry, can be off by 4 orders of magnitude. For this reason, we doubt errors in the numerical values of parameters in the model are responsible for the large discrepancy for m/z = 178, although they might partially explain the discrepancy. Instead we suspect the model must be completely missing key reaction(s) leading to an m/z=178 species.

Another possibility, hypothesis (ii.6), is that much of the m/z=178 signal observed from photolyzing $C_{10}H_7I$ in the presence of C_2H_2 is from C_4H_3I rather than $C_{14}H_{10}$. Because iodo compounds have much larger PICS than hydrocarbons, even a small amount of C_4H_3I formation could explain this mysterious m/z=178 peak. We tested this hypothesis with an iodine-free control experiment: we photolyzed 1-bromonaphthalene at 800 K and 25 Torr in the presence of acetylene. As shown in Figure S21a, m/z = 178 signal was not observed to be significant, while m/z = 152 ($C_{12}H_8$) and m/z = 153 ($C_{12}H_9$) were observed as expected. This indicates that the large m/z = 178 signal observed using $C_{10}H_7I$ as the radical precursor is an artifact related to the presence of iodine atoms in our system. We think mostly likely the m/z = 178 is due to formation of C_4H_3I, though this is not the only possible explanation (e.g. instead, presence of iodine could somehow catalyze formation of $C_{14}H_{10}$. Our models do not predict such catalysis nor significant formation of C_4H_3I, see section 4.11 in Supplementary Information. Also, we couldn't observe C_4H_3Br which we expect to see instead of C_4H_3I from the control experiment using 1-bromonapthalene with acetylene (Figure S22). So we don't understand the origin of this apparent artifact. If the presence of iodine in our system is somehow forming an artifact at m/z = 178 in the 1-iodonaphthalene experiments, it is possible that same artifact is occurring in the 2-iodonaphthalene experiments also, so there is uncertainty in the $C_{14}H_{10}$ yield. It is also plausible that C_4H_3I affects the observed time-dependent behavior of m/z = 178 in 2-naphthalenyl +

acetylene system at longer time scales. This is discussed further in the following subsection.

We conclude discrepancy (ii) is due to iodine side-reactions not included in our models, probably mainly due to the formation of C_4H_3I.

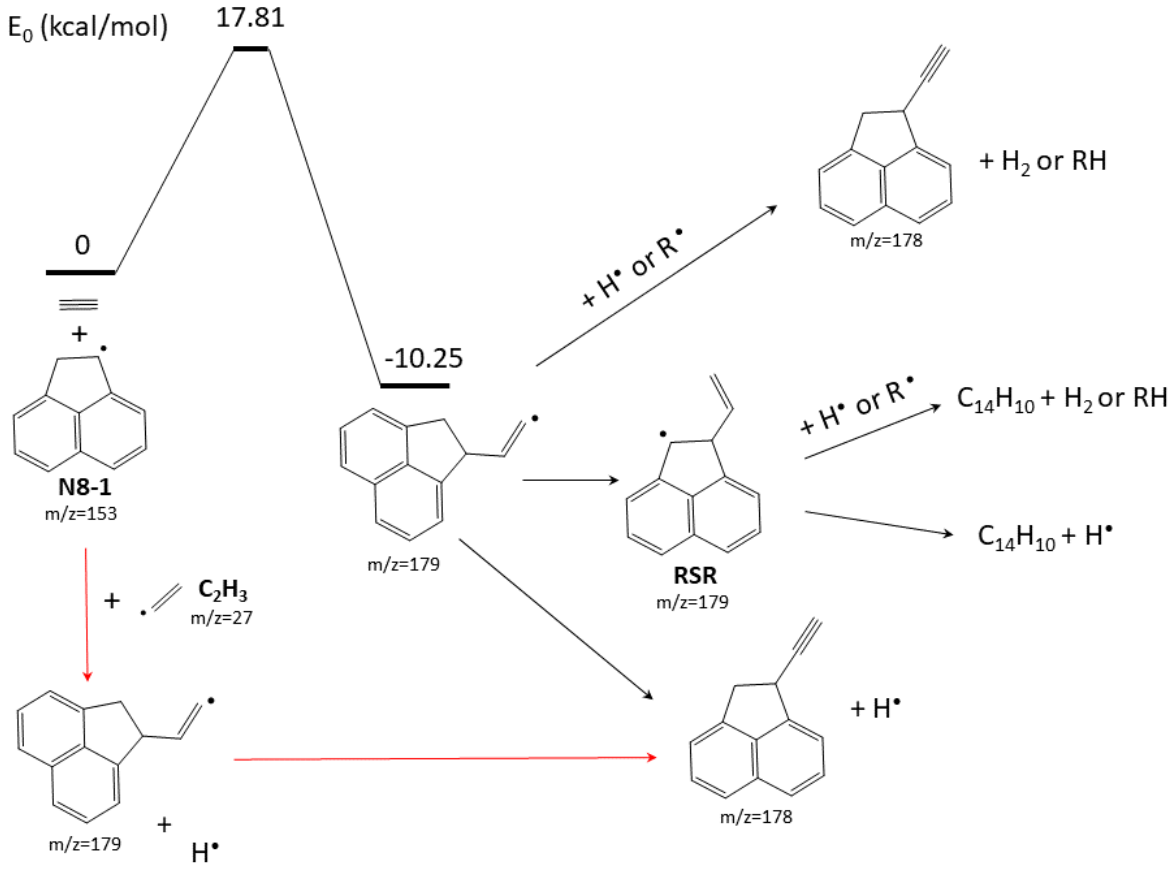

Figure S 18: Potential energy diagram for the secondary acetylene addition to N8-1 using the CBS-QB3 and suggested possible pathways to the formation of m/z = 178 species.

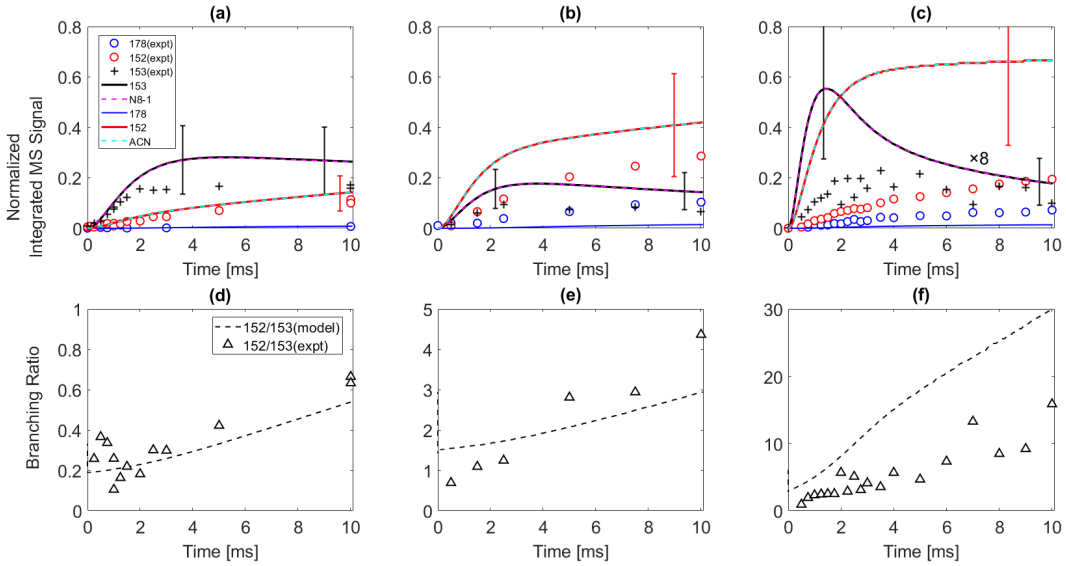

Figure S 19: Corresponding to Figure 2 in the main text. The kinetic model includes (i) intentionally reduced chemically activated rate of acenaphthylene formation (i.e. 1-naphthalenyl radical + C_2H_2 → ACN + H) by a factor of 5, (ii) N8-1 + C_2H_3 → m/z=178 + H_2, (iii) acenphthylene + C_2H_3→ m/z=178 + H (assumed $k = 1.62 \times 10^{10}\,\mathrm{cm^3\,mol^{-1}\,s^{-1}}$), and (iv) reactions indicated in Figure S18.

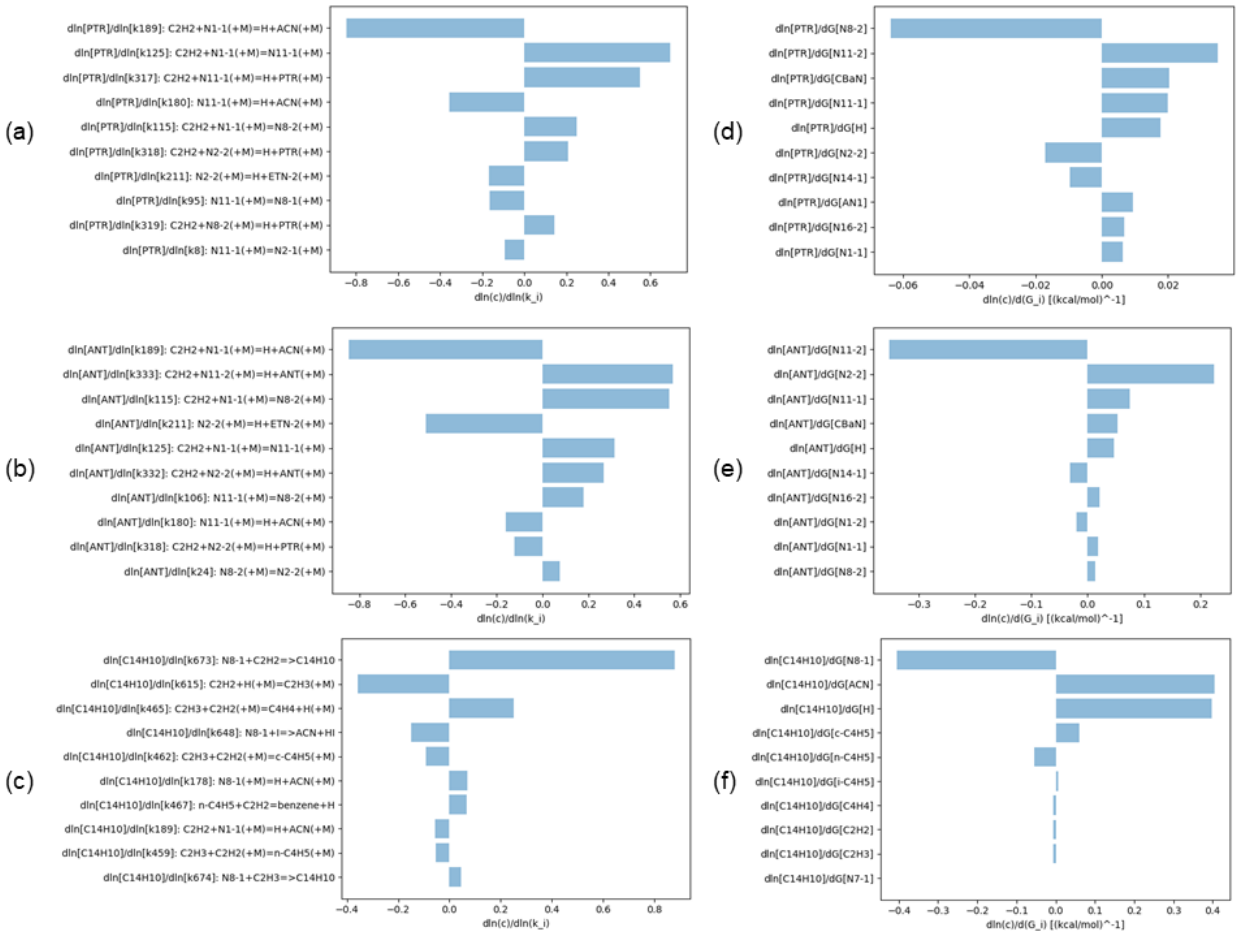

Figure S 20: Sensitivity analysis on phenanthrene to (a) rate coefficients and (d) thermochemistry; on anthracene to (b) rate coefficients and (e) thermochemistry; on $C_{14}H_{10}$ shown in Figure S18 to (c) rate coefficients and (f) thermochemistry ; Simulated under the condition of 800 K, 25 Torr, $[C_{10}H_7]_0 = 4.2 \times 10^{11}$ molecules cm^{-3}, $[C_2H_2] = 3{\times}10^{16}$ molecules/cm^3.

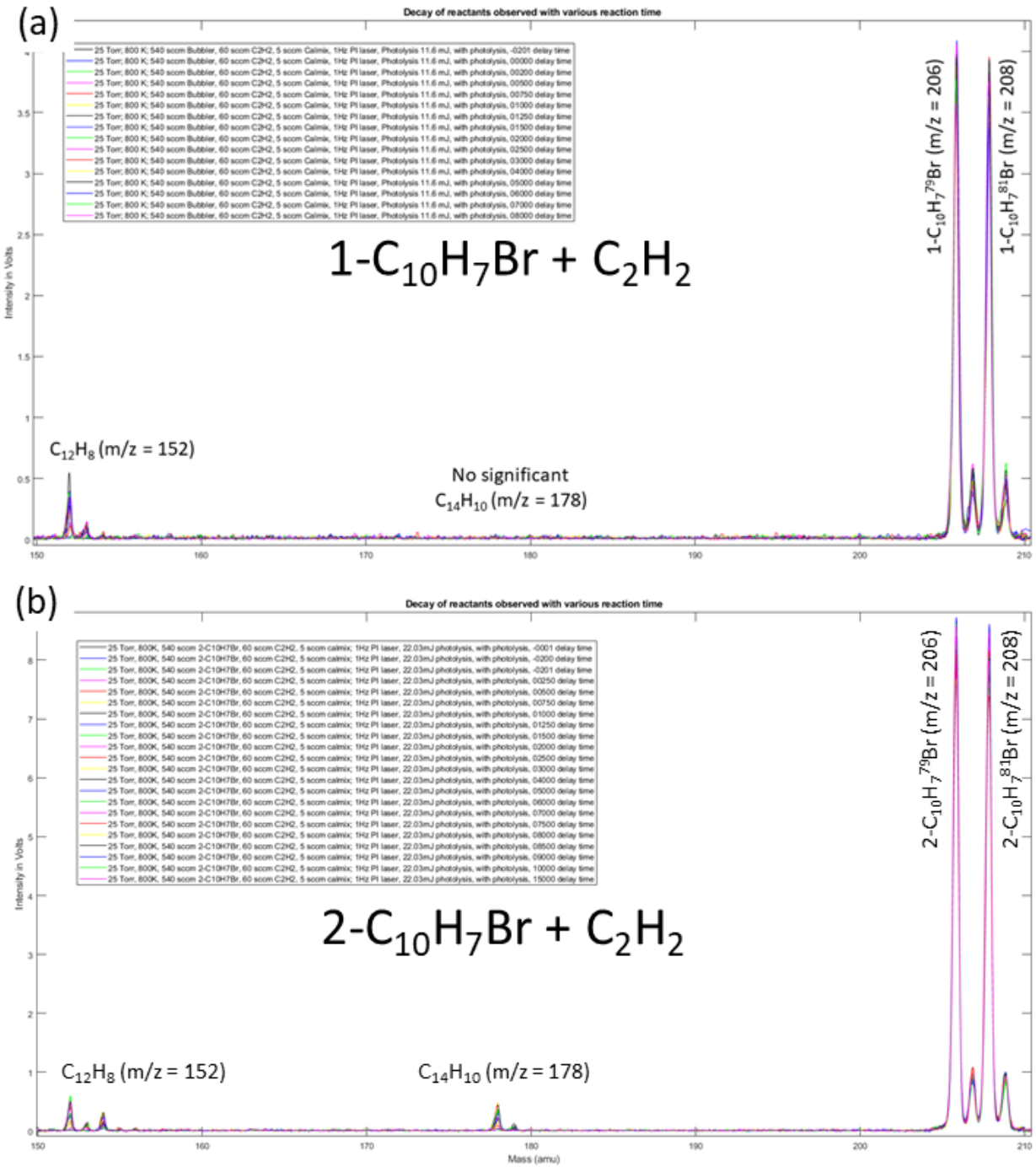

Figure S 21: Time-dependent Time-of-Flight mass spectrometry raw signals of the photolysis experiment on (a) 1-bromonaphthalene + acetylene measured up to 8 ms. Reactor condition was 800 K, 25 Torr, C_2H_2 concentration was 3×10^{16} molecules/cm^3, and (b) 2-bromonaphthalene + acetylene measured up to 15 ms. Reactor condition was 800 K, 25 Torr, C_2H_2 concentration was 3×10^{16} molecules/cm^3.

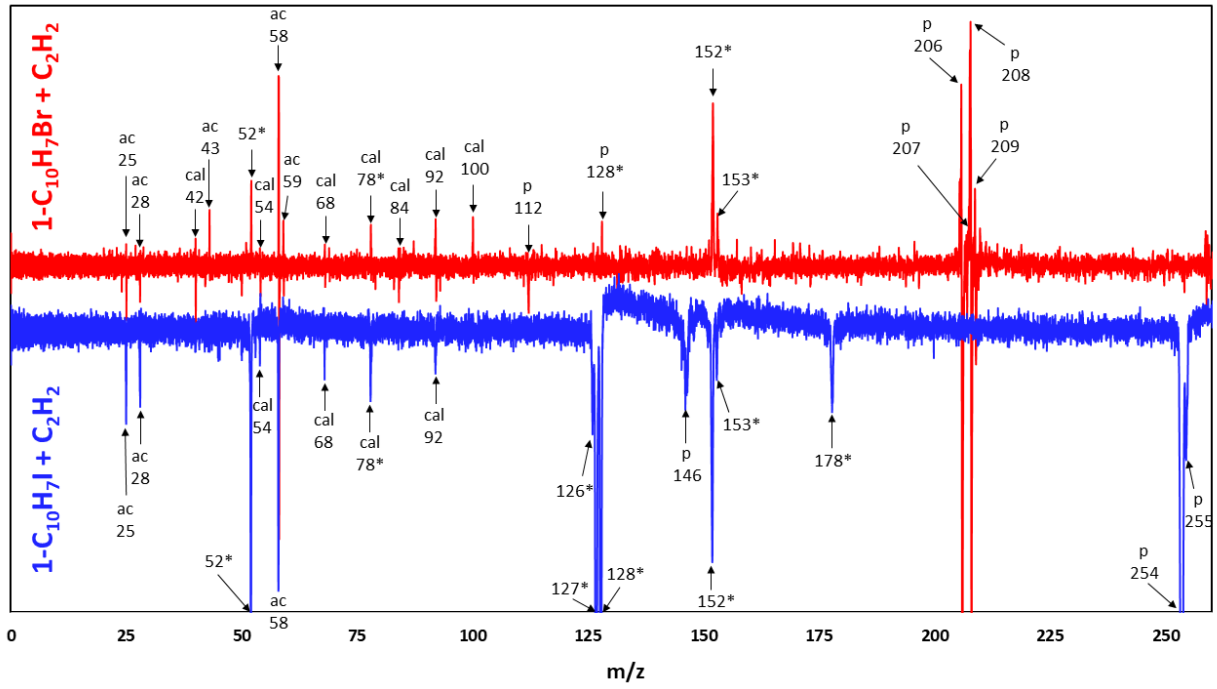

Figure S 22: Time-of-Flight mass spectrometry raw signals comparison between the photolysis experiment on 1-bromonaphthalene + acetylene (red) and 1-iodonaphthalene + acetylene (blue). Reactor conditions for both experiments were 800 K, 25 Torr, C_2H_2 concentration was 3×10^{16} molecules/cm^3. Each raw mass spectra is the subtraction between corresponding mass spectra at 8 ms and -200 us. By doing this, we can easily figure out which m/z signals originate from the reactions after the photolysis. The numbers in the figure indicates the m/z of each peak. 'ac' indicates that the corresponding peak is from acetylene residual; 'p' indicates that the corresponding peak is from the precursor used in each experiment (red peaks with 'p': from 97% purity 1-bromonaphthalene precursor; blue peaks with 'p': from 97% purity 1-iodonaphthalene precursor); 'cal' indicates that the corresponding peak is from calibration gases; Asterisk indicates that the corresponding peak is from the reactions after the photolysis.

4.6. Possibility of isomerization between 1- and 2-naphthalenyl radical

Since the residual energy after photolysis can possibly trigger unintentional isomerization between 1-naphthalenyl radical and 2-naphthalenyl radical, a simple assessment of this isomerization has been carried out using RRKM theory[12]. The dissociation energy of the 1-iodonaphthalene precursor to form I atom and 1-naphthalenyl radical is 2.795 eV (Ref. 16), while the photolysis laser pulses in this study contains 4.606 eV per photon.[17] Assuming all the residual energy (1.811 eV) stays in the 1-naphthalenyl radical after photolysis, parallel translation of the Boltzmann distribution of 1.811 eV from the ground state has been assumed. The external rotational terms for both reactant and transition state when using RRKM theory were ignored. The collision frequency coefficient was calculated using the sum of the radii of acetylene and benzene as the diameter of the target molecules. The collision frequency was calculated by multiplying the number density of total gas molecules under our experimental conditions. This turned out to be around $2.67 \times 10^8\,\mathrm{s}^{-1}$. Quantum chemical information for 1-naphthalenyl radical and the transition state for isomerization to 2-naphthalenyl radical have been taken from the literature.[18] The density of states and sum of states have been calculated using Beyer-Swinehart algorithm[19]. As a result, the normalized probability at the energy in which the isomerization rate coefficient is equal to the collision frequency was below 10^{-13}, as shown in Figure S23. This implies that under our experimental conditions, it is reasonable to ignore the effect of isomerization between 1-naphthalenyl radical and 2-naphthalenyl radical.

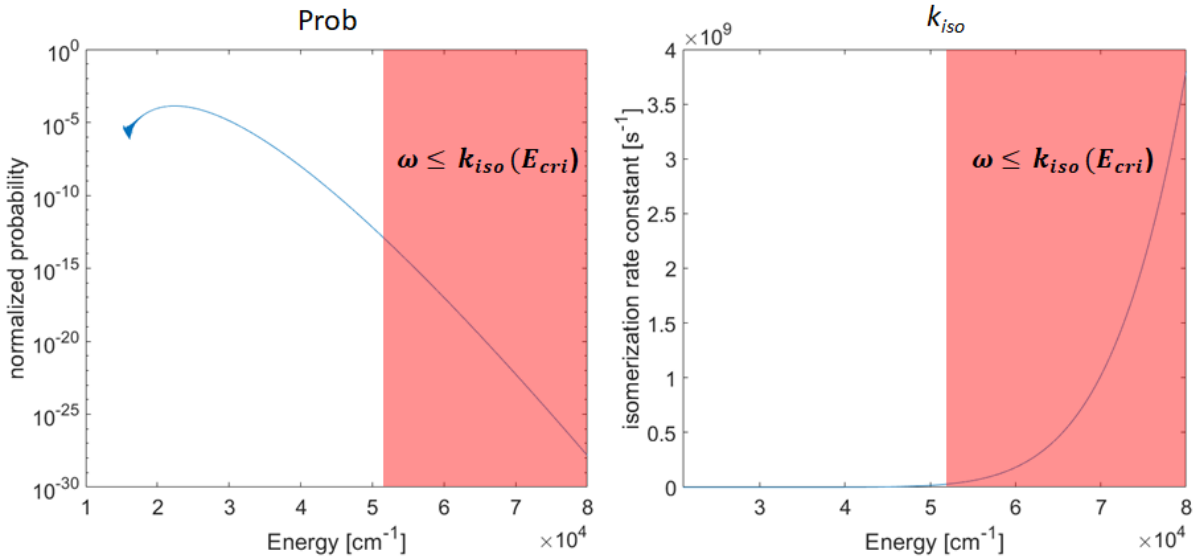

Figure S 23: RRKM calculation of 1- and 2-naphthalenyl radical isomerization. The left figure is the population profile with regard to the energy states of 1-naphthalenyl radical well. The right figure shows the corresponding isomerization rate constant at each energy state of the 1-naphthalenyl radical well. The red shaded region indicates the conditions where the isomerization rate constant is faster than the collision frequency.

4.7. Possibility of C_4H_3I as a source of m/z = 178 observation in 1-naphthalenyl + C_2H_2 system

C_4H_4 (m/z = 52) is a source for C_4H_3 radicals (m/z = 51) that later react with I atoms to form C_4H_3I (m/z = 178). Since I-atom containing species usually have high PICS, even small concentration of C_4H_3I can result in a significant m/z=178 signal in these photoionization experiments. To assess this possibility, additional kinetic modeling was carried out. On top of the kinetic model used in this study, following rate coefficients were added: $C_4H_4+H \rightarrow C_4H_3+H_2$ with k=4.0 × 10^{11} $cm^3\,mol^{-1}\,s^{-1}$ [20]; $C_4H_4+C_2H_3 \rightarrow C_4H_3+C_2H_4$ with k=4.0 × 10^{11} $cm^3\,mol^{-1}\,s^{-1}$ (assuming same as $C_4H_4 + H \rightarrow C_4H_3 + H_2$); $C_4H_3 + I \rightarrow C_4H_3I$ with k=1.0 × 10^{13} $cm^3\,mol^{-1}\,s^{-1}$. Unfortunately, even assuming the PICS of C_4H_3I as 50 Mb, the kinetic model indicated insignificant contribution of C_4H_3I into m/z = 178 signal observed from the experiments.

4.8. Sensitivity analyses on the yield of phenanthrene and anthracene to rate coefficients at various temperature conditions (2-naphthalenyl + C_2H_2 system)

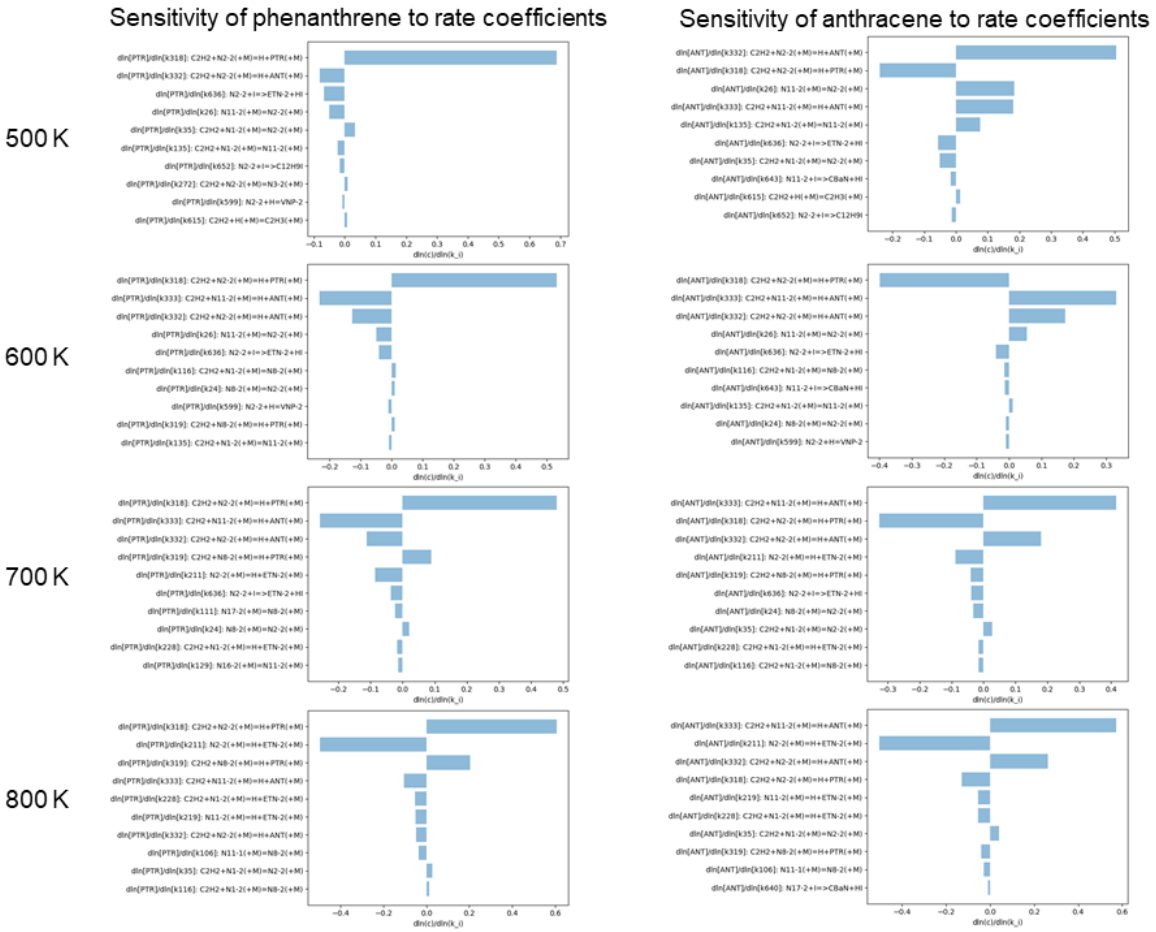

Figure S 24: Sensitivity analysis on phenanthrene (left column) and anthracene (right column) in 2-naphthalenyl + C_2H_2 system. Each row represents corresponding temperature; Detailed experimental conditions to each corresponding temperature are same as Figure 4 in the main text.

4.9. *Sensitivity analyses on the yield of 2-ethynylnaphthalene to rate coefficients at various temperature conditions (2-naphthalenyl + C_2H_2 system)*

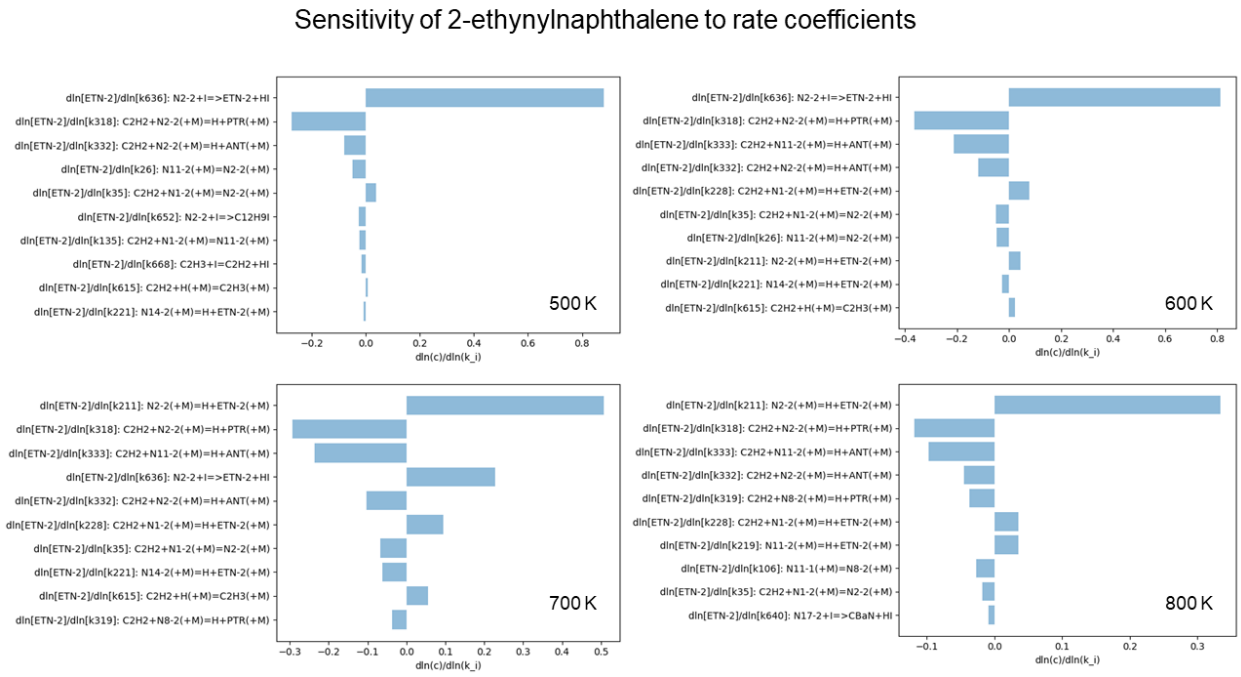

Figure S 25: Sensitivity analysis on 2-ethynylnaphthalene in 2-naphthalenyl + C_2H_2 system. Detailed experimental conditions to each corresponding temperature are same as Figure 4 in the main text.

4.10. Additional kinetic model included model simulation on 2-naphthalenyl + C_2H_2

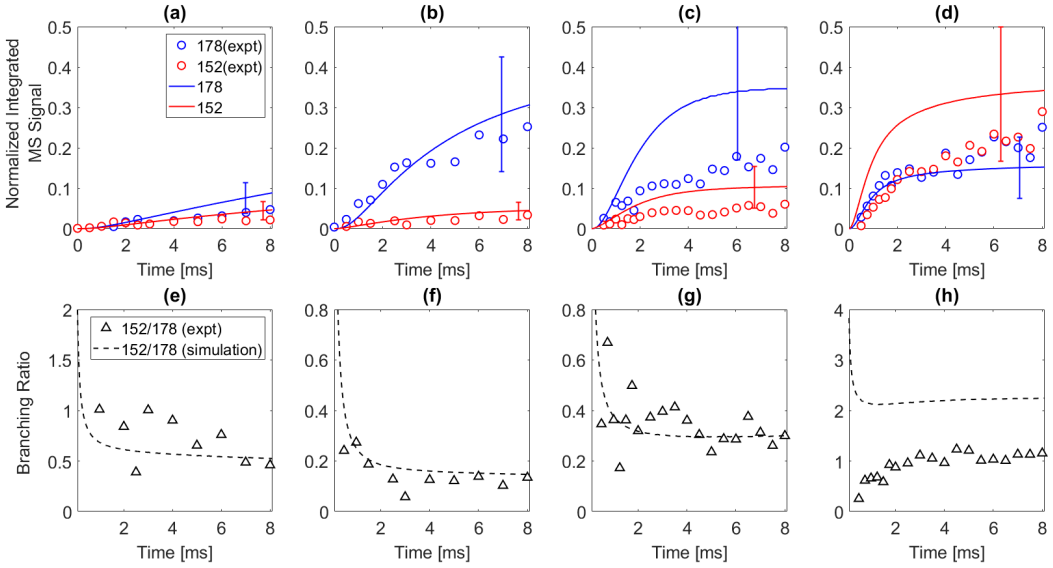

Figure S 26: Corresponding to Figure 4 in the main text. The kinetic model includes (i) intentionally reduced chemically activated rate of β-scission to form 2-ethynylnapthalene (i.e. N2-2 $\rightarrow$ ETN-2 + H) by a factor of 5, (ii) intentionally reduced N2-2 + I $\rightarrow$ ETN-2 + HI by a factor of 2, and (iii) intentionally reduced N2-2 + C_2H_2 $\rightarrow$ PTR + H by a factor of 5

4.11. Time-dependent integrated mass-spec signals result from 2-bromonaphthalene + C_2H_2 experiment

Since 2-naphthalenyl + C_2H_2 system also uses 2-iodonaphthalene as a precursor, it is plausible that C_4H_3I has an effect on the observed time-dependent behavior of m/z = 178 in 2-naphthalenyl + acetylene system after the secondary chemistry (e.g. $C_2H_2 + H \rightarrow C_2H_3$). We tested this hypothesis using 2-bromonaphthalene as a precursor. We photolyzed 2-bromonaphthalene at 800 K and 25 Torr in the presence of acetylene. Since bromine atom is not detectable in our photoionization time-of-flight mass spectrometry, using bromonaphthalene as a precursor has a disadvantage when it comes to estimation on both the initial $C_{10}H_7$ radical concentration and the sampling time that are necessary for kinetic modeling. However, different from iodine (m/z = 127), bromine (m/z = 79 and 81) doesn't overlap with 1- and 2-naphthalenyl radical (m/z = 127). So, it is clear that any observed m/z = 178 signal is solely attributed to $C_{14}H_{10}$ species.

From Figure S21b, we can observe m/z = 178 signal as it is expected in the model simulation. So it is clear to say that $C_{14}H_{10}$ is formed by acetylene addition to 2-naphthalenyl radical ($C_{10}H_7$). Also, from Figure S27a, the m/z = 178 signal shows stagnant time-dependent behavior after 2 ms as expected in the model simulation. It has to be noted that the sampling time is unknown from bromonaphthalene + C_2H_2 experiment. However, it is clear that m/z = 178 doesn't increase any further after 2 ms, which indicates that somehow formed C_4H_3I at the temperature above 700 K is a strong candidate for the discrepancy on m/z = 178 signal increasing behavior at longer time scale as shown in Figure 4c and d. From these, we conclude it is likely that discrepancy (iv) is mainly due to C_4H_3I formation in the system.

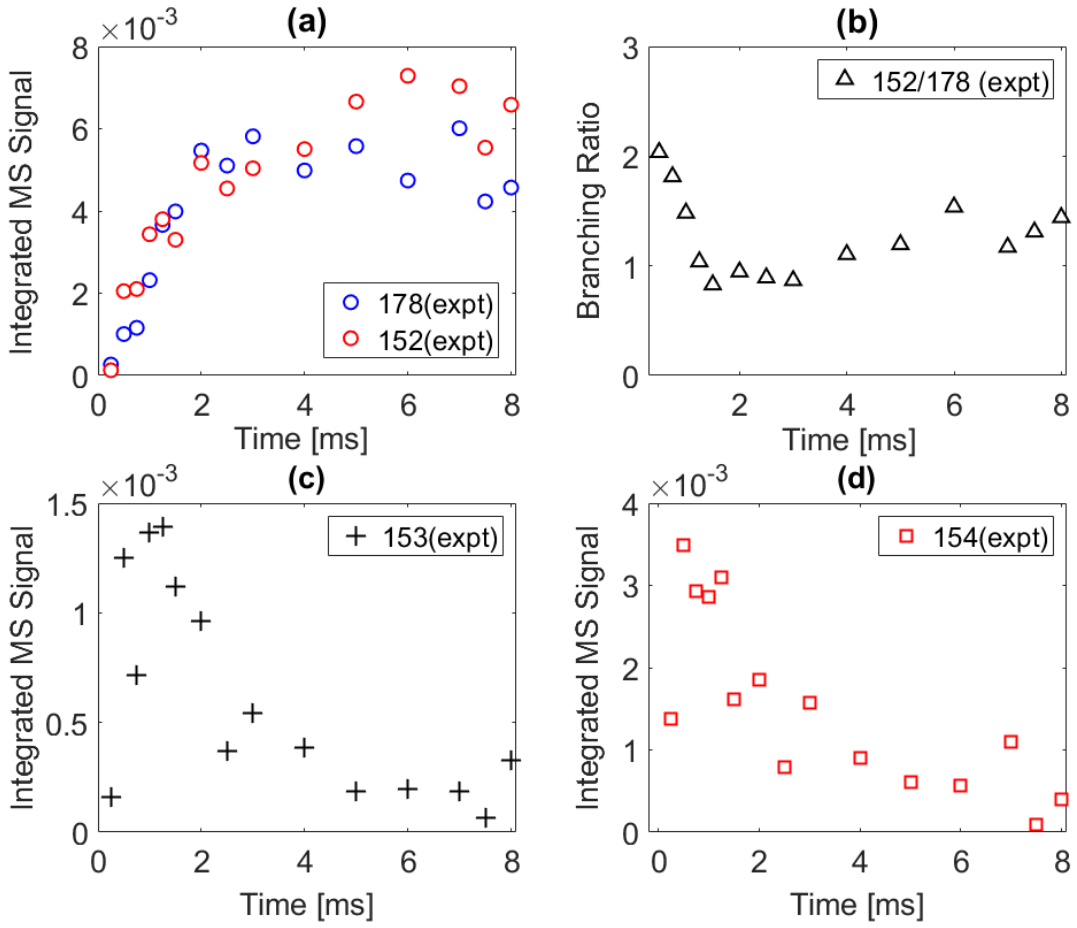

Figure S 27: Time-dependent integrated m/z signals measured up to 8 ms after the photolysis of the 2-bromonaphthalene in the presence of C_2H_2. Red open circles indicate the m/z = 152 signal; blue open circles indicate m/z = 178 signal; black cross symbols (+) indicate the m/z = 153 signal; red open square symbols indicate the m/z = 154 signal; and black open triangle symbols indicate the ratio of m/z = 152 to m/z = 178 from the experiment. Reactor conditions: 800 K, 25 Torr, and the concentration of C_2H_2 was 3×10^{16} molecules/cm^3.

4.12. $C_{14}H_{11}$ potential energy surface for Scheme 2

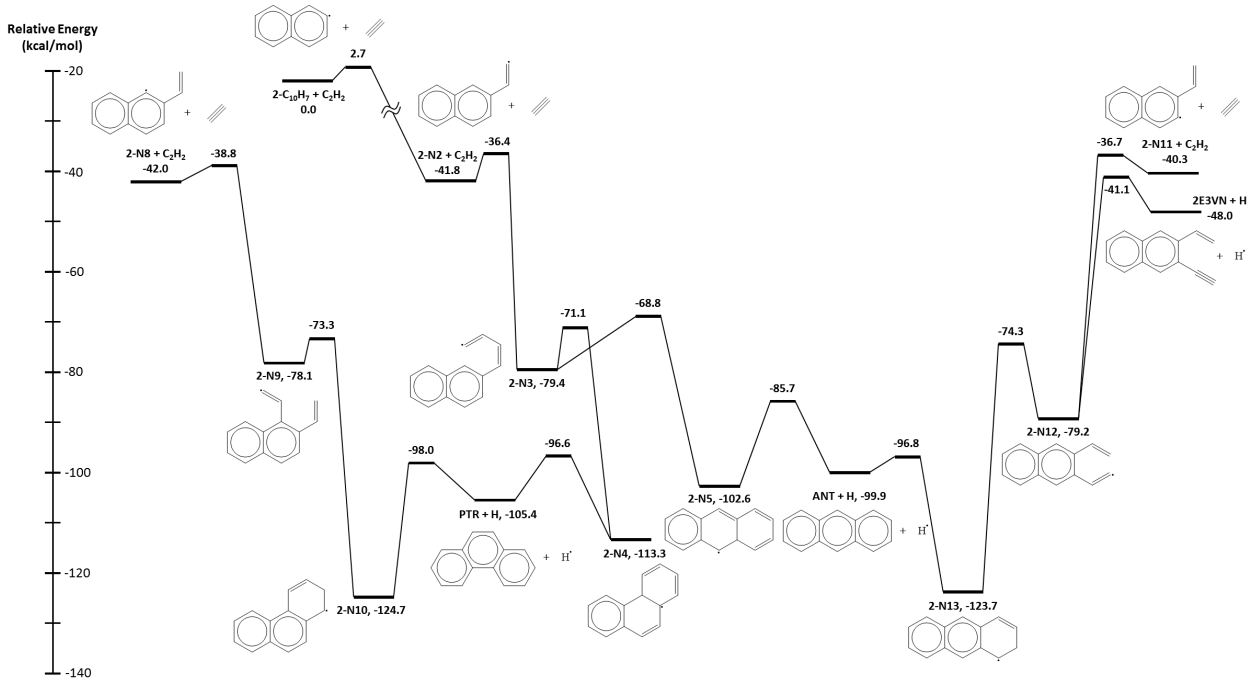

Figure S 28: This figure has been taken from Figure 3 in [13] and modified. The level of theory is G3(MP2,CC)//B3LYP/6-311G**. Energies are relative to 2-naphthalenyl radical + 2 C_2H_2

References

1. Klasinc L, Kovac B, Gusten H. Photoelectron spectra of acenes. Electronic structure and substituent effects. *Pure and Applied Chemistry* 1983;55(2):289–98. doi:10.1351/pac198855020289.

2. Lias SG. Ionization Energy Evaluation. 2017. URL: doi: https://doi.org/10.18434/T4D303. doi:https://doi.org/10.18434/T4D303.

3. Ismail H, Paul A, Green W, Askar F, Leonard J, Adam K, Judit Z, Giovanni M, Talitha S, David O, Craig T. Temperature-dependent kinetics of the vinyl radical (c2h3) self-reaction. *J Phys Chem A,* 2008;113(7):1278–86. doi:10.1021/jp8096132.

4. Wakamatsu H, Hidaka Y. Shock-tube and modeling study of chloroethane pyrolysis and oxidation. *International Journal of Chemical Kinetics* 2007;40(7):320–39. doi:10.1002/kin.20313.

5. Cool T, Wang J, Nakajima K, Taatjes C, Mcllroy A. Photoionization cross sections for reaction intermediates inhydrocarbon combustion. *International Journal of Mass Spectrometry* 2005;247(1-3):18–27. URL: https://doi.org/10.1016/j.ijms.2005.08.018. doi:10.1063/1.2010307.

6. Yang B, Wang J, Cool TA, Hansen N, Skeen S, Osborn DL. Absolute photoionization cross-sections of some combustion intermediates. *Int J Mass Spectrom* 2012;309:118–28.

7. Kanno N, Tonokura K. Vacuum ultraviolet photoionization mass spectra and cross-sections for volatile organic compounds at 10.5 ev. *applied spectroscopy* 2007;61(8):896–902. URL: https://journals.sagepub.com/doi/10.1366/000370207781540033. doi:10.1366/000370207781540033.

8. Zhou Z, Xie M, Wang Z, Qi F. Determination of absolute photoionization cross-sections of aromatics and aromatic derivatives. *Rapid Commun Mass Spectrom* 2009;23:3994–4002. doi:10.1002/rcm.4339.

9. Gans B, Mendes LAV, Boye-Peronne S, Douin S, Garcia G, Soldi-Lose H, de Miranda BKC, Alcarz C, Carrasco N, Pernot P, Gauyacq D. Determination of the absolute photoionization cross sections of ch3 and i produced from a pyrolysis source, by combined synchrotron and vacuum ultraviolet laser studies. *J Phys Chem A* 2010;114:3237–46. URL: https://doi.org/10.1021/jp909414d. doi:10.1051/0004-6361:20040541.

10. C.E.Brion , M.Dyck , G.Cooper . Absolute photoabsorption cross-sections (oscillator strengths) for valence and inner shell excitations in hydrogen chloride, hydrogen bromide and hydrogen iodide. *Journal of Electron Spectroscopy and Related Phenomena* 2005;114-147:127–30. URL: https://doi.org/10.1016/j.elspec.2005.01.010. doi:10.1051/0004-6361:20040541.

11. Smith MC, Zhu G, Buras ZJ, Chu TC, Yang J, Green WH. Direct measurement of radical-catalyzed c6h6 formation from acetylene and validation of theoretical rate coefficients for

c2h3 + c2h2 and c4h5 + c2h2 reactions. *J Phys Chem A* 2020;124(14):2871–84. URL: http://doi.wiley.com/10.1002/ange.201404537. doi:10.1021/acs.jpca.0c00558.

12. Marcus RA. Unimolecular dissociations and free radical recombination reactions. *J Chem Phys* 1952;20(3):359–64. URL: https://doi.org/10.1063/1.1700424. doi:10.1063/1.1700424.

13. Chu TC, Smith MC, Yang J, Liu M, Green WH. Theoretical study on the haca chemistry of naphthalenyl radicals and acetylene: the formation of c12h8, c14h8, and c14h10 species. *Int J Chem Kinet* 2020;52:752–68. doi:10.1002/kin.21397.

14. Grinberg Dana A, Ranasinghe D, Wu H, Grambow C, Dong X, Johnson M, Goldman M, Liu M, Green W. Arc - automated rate calculator, version 1.1.0. https://github.com/ReactionMechanismGenerator/ARC; 2019. doi:10.5281/zenodo.3356849.

15. Frisch MJ, Trucks GW, Schlegel HB, Scuseria GE, Robb MA, Cheeseman JR, Scalmani G, Barone V, Petersson GA, Nakatsuji H, Li X, Caricato M, Marenich AV, Bloino J, Janesko BG, Gomperts R, Mennucci B, Hratchian HP, Ortiz JV, Izmaylov AF, Sonnenberg JL, Williams-Young D, Ding F, Lipparini F, Egidi F, Goings J, Peng B, Petrone A, Henderson T, Ranasinghe D, Zakrzewski VG, Gao J, Rega N, Zheng G, Liang W, Hada M, Ehara M, Toyota K, Fukuda R, Hasegawa J, Ishida M, Nakajima T, Honda Y, Kitao O, Nakai H, Vreven T, Throssell K, Montgomery Jr. JA, Peralta JE, Ogliaro F, Bearpark MJ, Heyd JJ, Brothers EN, Kudin KN, Staroverov VN, Keith TA, Kobayashi R, Normand J, Raghavachari K, Rendell AP, Burant JC, Iyengar SS, Tomasi J, Cossi M, Millam JM, Klene M, Adamo C, Cammi R, Ochterski JW, Martin RL, Morokuma K, Farkas O, Foresman JB, Fox DJ. Gaussian˜16 Revision C.01. 2016. Gaussian Inc. Wallingford CT.

16. Lifshitz A, Tamburu C, Dubnikova F. Reactions of 1-naphthyl radicals with ethylene. single pulse shock tube experiments, quantum chemical, transition state theory, and multiwell calculations. *J Phys Chem A* 2008;112(5):925–33. URL: https://pubs.acs.org/doi/pdf/10.1021/jp077289s. doi:10.1021/jp077289s.

17. Middaugh JE, Buras ZJ, Matrat M, Chu TC, Kim YS, Alecu IM, Vasiliou AK, Goldsmith CF, Green WH. A combined photoionization time-of-flight mass spectrometry and laser absorption spectrometry flash photolysis apparatus for simultaneous determination of reaction rates and product branching. *Rev Sci Instrum* 2018;89(7):074102. URL: http://dx.doi.org/10.1063/1.5024399. doi:10.1063/1.5024399.

18. Mebel A, Georgievskii Y, Jasper A, Klippenstein S. Temperature- and pressure-dependent rate coefficients for the haca pathways from benzene to naphthalene. *Proceedings of the Combustion Institute* 2016;36(1):919–26. URL: https://doi.org/10.1016/j.proci.2016.07.013. doi:10.1016/j.proci.2016.07.013.

19. Beyer T, Swinehart D. Algorithm 448: Number of multiply-restricted partitions [a1]. *Communications of the ACM* 1973;16(6):379. URL: https://doi.org/10.1145/362248.362275. doi:10.1145/362248.362275.

320 20. Ghibaudi E, Colussi AJ. Kinetics and Thermochemistry of the Equilibrium 2(Acetylene) = Vinylacetylene. Direct Evidence Against a Chain Mechanism. *The Journal of Physical Chemistry* 1988;92(20):5839–42. URL: https://pubs.acs.org/doi/pdf/10.1021/j100331a058. doi:10.1021/j100331a058.